Towards a Reduced-Scaling Method for Calculating Coupled Cluster Response Properties

Ashutosh Kumar

Dissertation submitted to the Faculty of the

Virginia Polytechnic Institute and State University

in partial fulfillment of the requirements for the degree of

Doctor of Philosophy

in

Literature and Technology

T. Daniel Crawford, Chair

Eduard Valeyev

Diego Troya

Alan Esker

May 9, 2018

Blacksburg, Virginia

Keywords: Coupled Cluster, Reduced-Scaling, Response Properties

Copyright 2018, Ashutosh Kumar

Towards a Reduced-Scaling Method For Calculating Coupled Cluster Response Properties

Ashutosh Kumar

(ABSTRACT)

One of the central problems limiting the application of accurate *ab initio* methods to large molecular systems is their high computational costs, i.e., their computing and storage requirements exhibit polynomial scaling with the size of the system. For example, the coupled cluster method — the "gold standard" of quantum chemistry — scales as $\mathcal{O}(N^6)$, where N is a measure of the system size. Local correlation techniques, however, have the potential to alleviate this scaling problem. While these methods have been quite successful in describing correlation energies they perform rather poorly for response properties like dipole polarizabilities and optical rotation. In this work, we identify some of the reasons behind the failure of popular local correlation models like Frozen Virtual Natural Orbitals (FVNO) and Pair Natural Orbitals (PNO) in capturing the response of the wavefunction. Consequently,

we introduce novel modifications to these schemes which we call FVNO++ and PNO++ respectively. Initial results indicate that these techniques significantly outperform their conventional counterparts and can be used for calculating response properties of large molecular systems.

This work was supported by a grant (CHE-1465149) from the U.S. National Science Foundation. Advanced Research Computing Center at Virginia Tech provided the necessary computational resources and technical support for all the calculations reported here.

Acknowledgments

Contents

List of Figures

List of Tables

Chapter 1

Introduction

1.1 Chirality

Lord Kelvin was the first to use the word 'chiral' in his lecture at Oxford University in 1894: "I call any geometrical figure, or group of points, 'chiral', and say that it has chirality if its image in a plane mirror, ideally realized, cannot be brought to coincide with itself"[].

There are different ways in which a molecule could be chiral. The most common example being the presence of a chiral center like a carbon or nitrogen atom with four different substituents. Axial chirality, usually possessed by molecules with cumulated double bonds like allenes and chirality planes found in compounds like paracyclophanes are other popular examples of chiral elements found in nature.

A chiral molecule and its mirror image are known as enantiomers. Although the enantiomers

have idential phyical properties like boiling and melting points their interactions in a chiral environment can be quite different. For example, while the (R) enantiomer of the compound limonene smells like lemons and oranges, as the name sugggests, the (S) enantiomer on the other hand smells like turpentine. Thus, the interaction of the (S) enantiomer with the chiral molecules constituting the olfactory receptors responsible for the sensation of smell is totally different from its fellow enantiomer. The enantiomers also interact differently with the left- and right-hand circularly polarized (LCP and RCP) light in processes of absorption, refraction, etc. A chiral molecule posesses the properties of circular dichroism (CD) and circular birefringence, i.e. it has different absorption coefficents and refractive indices for the LCP and RCP light, respectively. As a result of circular birefringence, the plane of polarization of a plane-polarized light in a chiral medium gets rotated/shifted by an amount known as the optical rotation of the medium. It should be noted that an enantiomeric pair of chiral molecules has equal magnitudes of optical rotation but in opposite directions.

Since almost every part of the human body is composed of chiral molecules, its unsurprising that more than 60% of the pharmaceutical drugs are chiral as well. Hence, one of the most important aspect of the drug-design research is to be able to define the absolute configuration (AC) of the chiral molecules in order to study their behaviour in biological systems as many biological activities are only associated with one specific AC. A very tragic example in this regard is that of the drug thalidomide which was originally prescribed to pregnant women in Europe in 1950s to cure morning sickness but resulted in birth-defects in thousands of infants. It was found through a study done on rodents that the (R) enantiomer is indeed a

sedative but the (S) enantiomer is a teratogen[]. Furthemore, these enantiomers were found to rapidly interconvert in vivo in humans[] because of which separating these two forms before use doesn't help.

The first step in experimental determination of AC either involves the separation of a racemic mixture (equal concentration of both the enantiomers) into individual enantiomers using chiral resolution methods like chiral column chromatography or a selective synthesis of a given enantiomer using the process of asymmetric synthesis. X-ray crystallography would then be the most popular procedure, provided one can crystallize the molecule first which usually requires the presence of heavy atom(s). Alternatively, one can measure the responses of the enantiomers like CD and optical rotation using corresponding chiroptical spectroscopy techniques like electronic and vibrational CD i.e. ECD (UV-VIS) and VCD (IR) and polarimetry, followed by comparision against some suitable reference chiral substrate. However, in cases of ambiguity regarding appropriate references, accurate *ab initio* methods can come to the rescue and help validate these experimental measurements. Furthermore, designing an asymmteric synthesis might not be straightforward for many chiral systems, especially the ones with large number of stereocenters. In such cases, theory can even take the lead and predict the corresponding AC. In other words, theoretical calculations of these chiroptical properties could serve as a very useful computational tool for modern organic chemists. In particular, accurate optical rotation calculations are highly desired as the experimental techniques for measuring this property are fairly stable and robust in both gas and solution phases.

1.2 *Ab Initio* Optical Rotation Calculations

Rosenfeld developed a quantum mechanical recipe for calculating optical rotations in the year 1929[54]. He showed that in the presence of an external electromagnetic field, the induced dipole moment in a molecule can be written as:

$$\langle \vec{\mu} \rangle = \boldsymbol{\alpha} \vec{E} + \frac{1}{\omega} \mathbf{G}' \frac{\partial \vec{B}}{\partial t} \tag{1.1}$$

where $\vec{E}$ and $\vec{B}$ are the time dependent electric and magnetic field vectors respectively, ω is the frequency of the filed, α is the electric dipole polarizability tensor and the $\mathbf{G}'$ tensor, also known as the Rosenfeld tensor is associated with the property of optical rotation. Invoking time-dependent Schrödinger's equation in conjunction with perturbation theory, expanding the expectation value of dipole operator in orders of perturbation and identifying the term linear in $\vec{E}$ and $\frac{\partial \vec{B}}{\partial t}$, for exact states, the $\boldsymbol{\alpha}$ and $\mathbf{G}'$ tensor look like,

$$\begin{aligned} \boldsymbol{\alpha}(\omega) &= -\frac{2}{\hbar} \sum_{n \neq 0} \frac{\omega_{no} \langle \psi_o | \vec{\mu} | \psi_n \rangle \langle \psi_n | \vec{\mu} | \psi_o \rangle}{{\omega_{no}}^2 - \omega^2} \\ \mathbf{G}'(\omega) &= -\frac{2}{\hbar} \mathrm{Im} \sum_{n \neq 0} \frac{\omega \langle \psi_o | \vec{\mu} | \psi_n \rangle \langle \psi_n | \vec{m} | \psi_o \rangle}{{\omega_{no}}^2 - \omega^2} \end{aligned} \tag{1.2}$$

Here, $\vec{\mu}$ and $\vec{m}$ are electric and magnetic dipole operators, $\vec{\mu} = \sum_i q_i \vec{r_i}$ and $\vec{m} = \sum_i \frac{q_i}{2m_i} \vec{r_i} \times \vec{p_i}$, ω is the frequency of light, ω_{no} is the excitation energy of the state ψ_n. Im means the imaginary part of the equation and the summation runs over all the excited states ψ_n. Specific

rotation, $[\alpha]_\omega$ is related to the trace of the Rosenfeld tensor normalized by pathlength and concentration and is usually reported in the units of deg $dm^{-1}(g/mL)^{-1}$,[14]

$$[\alpha]_\omega = \frac{(72.0 \times 10^6)\hbar^2 N_A\, \omega}{c^2 {m_e}^2 M} \times \left[\frac{1}{3} Tr(\mathbf{G}')\right] \tag{1.3}$$

Here, $\mathbf{G}'$ and ω are in atomic units, c is the speed of light (m/s), m_e is the mass of electron (kg), M is the molecular mass (amu) and N_A is Avogadro's number. Calculating the $\mathbf{G}'$ tensor using equation (1.2) requires explicit calculations of a large number of excited states which is computationally prohibitive. A more practical approach is to invoke the response formalism [32, 30], which casts these tensors as response functions,

$$\begin{aligned} \boldsymbol{\alpha}(\omega) &= \langle\langle \vec{\mu}; \vec{\mu} \rangle\rangle \\ \mathbf{G}'(\omega) &= -\mathrm{Im}\langle\langle \vec{\mu}; \vec{m} \rangle\rangle \end{aligned} \tag{1.4}$$

The response theory focuses on the perturbation of the ground state wavefunction in the presence of an external field, avoiding explicit calculations of excited states. Polavarapu was the first to use this theory to calculate *ab initio* specific rotations of molecules using time dependent Hartree Fock (TDHF) method [50]. The signs of the calculated values matched with that of the experiment for most of his structures, while their magnitudes differed generally by a factor of two. Inspired by Polavarapu's success, Cheeseman et al. [9, 64] included correlation effects in these calculations by using TD-DFT. Using large basis sets with diffuse functions like aug-cc-pVDZ and aug-cc-pVTZ,[19] they were able to match the experimental values very closely, with a deviation of 20-25 degrees for a set of 28 chiral molecules. Ruud

et al. extended the calculations to the coupled cluster level using coupled cluster response theory developed by Koch and Jørgensen[32], and obtained very promising results[57]. Unsurprisingly, these response based simulations have been used as an accurate and reliable tool in the process of determining the AC of a large number of chiral molecules[33]. However, all these calculations were done on single isolated molecules and thus ideally they should only be expected to match vapor phase optical rotation (OR) which can be measured by using cavity ring down spectrometry, thanks to the pioneering works of Vacaaro and co-workers.[] Thus, in order to match the solution phase OR measurements, the response theory needs to be combined with accurate solvation models.

However, works in this regard, as shown in chapter 2 of this manuscript have been less than satisfactory and the only robust way of accounting for solvent effects seem to be including the solvent molecules explicitly in the QM calculations. Since rotation is a dynamic property, one needs to average OR values over several configurations or snapshots (obtained by molecular dynamics (MD) simulations) to be able to match experimental values. Multiple calculations coupled with the polynomical scaling of coupled cluster (CC) methods, puts a heavy burden on the computational resources. An obvious way to make these compuations practical is to seek the help of CC reduced-scaling techniques like projected natural orbitals (PNO) approach[] which has been really sucessfull in describing energetics of large molecular systems. However, works towards the extension of these methods to calculate chiroptical properties has been fairly limited[]. McAlexander and Crawford in their recent work[] demonstrated that the regular PNO approach suffers from slow convergence towards

the full canonical result. The main focus of this work is identifying the reasons behind the sub-optimal peformance of such approaches for optical rotations. Subsequently, novel modifications have been proposed which significantly improves the performance of these schemes. The necessary equations to calculate chiroptical properties within CC linear response theory are derived in Chapter 2. Also, a brief description of solvation models that have been used for modeling chiroptical properties is provided. Chapter 3 investigates the performance of natural orbitals (FVNO scheme) for CC dynamaic polarizabilites. A new scheme called FVNO++ is developed in chapter 4 which significantly outperforms the regular FVNO scheme for both polarizabilities and rotations. Chapter 5 extends the FVNO++ (a reduced-prefactor) approach to the reduced-scaling domain by implementing what we call as PNO++ method. Finally, concluding remarks are given in Chapter 6.

Chapter 2

Coupled Cluster Response Theory

2.1 Theoretical tools

The most basic problem in quantum mechanics is to solve the time independent non-relativistic Schrödinger equation [58]. It can be solved exactly for one electron hydrogen-like species and only approximate solutions can be obtained for many electron systems. Under the Born-Oppenheimer approximation[8], the Hartree-Fock (HF) theory[65] is one of the simplest approximation methods. The HF wavefunction is a single slater determinant of spin orbitals which naturally obeys the Pauli's antisymmetry principle. Since the energy expectation value of a slater determinant is a functional of the spin-orbitals, optimized spin orbitals can be obtained by minimizing this functional with respect to the orbitals by invoking the variational principle. This minimization procedure is usually coupled with the constraints of

an orthonormal basis using the Lagrangian method of undetermined multipliers. Finally, a set of non-linear equations are solved through a self consistent procedure, because of which HF is also called self consistent field theory (SCF). The HF method recovers up to 99% of the electronic energy but fails to take into account the electron correlation effects which constitute the remaining 1% and are very important for accurate calculations of properties. However, due to its simplicity it is usually the starting point for other correlation methods like the coupled cluster method.

Coupled cluster theory

Coupled cluster[15] (CC) theory is a very accurate electronic structure method that has been widely used in quantum chemistry. It takes into account the electron correlation effects by expressing the wavefunction as a linear combination of slater determinants within an exponential framework. This is achieved by the use of cluster operators $\hat{T}$ acting on the HF wavefunction.

$$|\Psi_{CC}\rangle = e^{\hat{T}}|\Psi_o\rangle, \tag{2.1}$$

where

$$\hat{T} = \hat{T}_1 + \hat{T}_2 + \hat{T}_3 + ... \hat{T}_n \tag{2.2}$$

$|\Psi_o\rangle$ is the reference wavefunction, usually taken as the HF wavefunction, and the $\hat{T}_1$ operator is the linear combination of all single excitation operators, which replace an occupied orbital in the HF wavefunction with a virtual orbital. It takes into account the relaxation of the one electron basis functions, i.e HF molecular orbitals, due to the correlation of the electronic motions. In second quantization[28] formalism, $\hat{T}_1$ can be written as :

$$\hat{T_1} = \sum_{ia} t_i^a \{a_a^\dagger a_i\} \tag{2.3}$$

where the indices i, j, k ... refer to occupied orbitals while the indices a, b, c ... refer to virtual spin orbitals. In the above equation, $a_a^\dagger$ is called the creation operator as it creates a new particle state (virtual orbital) when it acts on a slater determinant.

$$a_a^\dagger |\phi_b ... \phi_d\rangle = |\phi_a \phi_b ... \phi_d\rangle \tag{2.4}$$

a_i is the hermitian conjugate of the creation operator and is called the annihilation operator as it removes a hole state (occupied orbital) when it acts on a slater determinant.

$$a_i |\phi_i \phi_j ... \phi_l\rangle = |\phi_j ... \phi_l\rangle \tag{2.5}$$

The $\hat{T}_2$ operator is the linear combination of all double excitation operators. It correlates the motion of all pairs of electrons of the molecule and can be expressed in second quantization as:

$$\hat{T_2} = \frac{1}{4} \sum_{ijab} t_{ij}^{ab} \{a_a^\dagger a_b^\dagger a_j a_i\} \tag{2.6}$$

Similarly, the $\hat{T}_3$ operator correlates the motion of all triplets of electrons and so on. In general,

$$\hat{T_n} = \frac{1}{n!}^2 \sum_{ij..ab..}^{n} t_{ij..}^{ab..} \{a_a^\dagger a_b^\dagger ... a_j a_i\} \tag{2.7}$$

If we expand the exponential ansatz of the CC wavefunction,

$$|\Psi_{CC}\rangle = (1 + (\hat{T}_1 + \hat{T}_2 + \hat{T}_3 + ...) + \frac{1}{2!}(\hat{T}_1 + \hat{T}_2 + \hat{T}_3 + ...)^2 + ...)|\Psi_o\rangle \tag{2.8}$$

we get a linear combination of all possible Slater determinants, which makes CC wavefunction an exact wavefunction in the basis set limit, just like full configuration interaction. Thus, the full CC wavefunction is a solution of the Schrödinger equation.

$$\hat{H}e^{\hat{T}}|\Psi_o\rangle = E_{cc}\, e^{\hat{T}}|\Psi_o\rangle \tag{2.9}$$

On multiplying the above equation by the inverse of the exponential operator i.e $e^{-\hat{T}}$ and projecting it against the reference and excited determinants, we get the energy and the amplitude equations of coupled cluster theory.

$$\langle\Psi_o|e^{-\hat{T}}\hat{H}e^{\hat{T}}|\Psi_o\rangle = E_{cc} \tag{2.10}$$

$$\langle\Psi_{i.}^{a.}|e^{-\hat{T}}\hat{H}e^{\hat{T}}|\Psi_o\rangle = 0. \tag{2.11}$$

Here $\Psi_{i.}^{a.}$ can refer to any excited Slater determinant singles, doubles etc. The similarity transformed Hamiltonian $e^{-\hat{T}}\hat{H}e^{\hat{T}}$ also written as $\bar{H}$ can be expressed in the Hausdorf expansion [42]as:

$$e^{-\hat{T}}\hat{H}e^{\hat{T}} = \hat{H} + [\hat{H}, \hat{T}] + \frac{1}{2!}[[\hat{H}, \hat{T}], \hat{T}] + \frac{1}{3!}[[[\hat{H}, \hat{T}], \hat{T}], \hat{T}] + \frac{1}{4!}[[[[\hat{H}, \hat{T}], \hat{T}], \hat{T}], \hat{T}] + ... \tag{2.12}$$

Also, the second quantized form of the Hamiltonian can be written as[15]:

$$\hat{H} = \sum_{pq} h_{pq}\{a_p^\dagger a_q\} + \frac{1}{4}\sum_{pqrs}\langle pq||rs\rangle\{a_p^\dagger a_q^\dagger a_s a_r\} \tag{2.13}$$

Using the above two equations and the Wick's theorem[70], the coupled cluster energy equation gets simplified as:

$$E_{cc} = E_o + \sum_{ia} f_{ia} t_i^a + \frac{1}{4} \sum_{aibj} \langle ij||ab\rangle t_{ij}^{ab} + \frac{1}{2} \sum_{aibj} \langle ij||ab\rangle t_i^a t_j^b \tag{2.14}$$

The amplitudes t_i^a and t_{ij}^{ab} can be obtained by solving the coupled cluster amplitude equations. However, Full CC is computationally impractical and truncated CC methods like CCSD: $\hat{T} = \hat{T}_1 + \hat{T}_2$, CCSDT: $\hat{T} = \hat{T}_1 + \hat{T}_2 + \hat{T}_3$ are used. The CCSD(T)[60] method, which treats the triples approximately using perturbation theory is also a popular method. The exponential structure of the wavefunction makes the truncated CC methods more efficient compared to that of the linear CI methods. CCSD wavefunction implicitly includes the triples and quadruples excitation contributions to its singles and doubles amplitude equations because of the products of cluster operators like $\hat{T}_1\hat{T}_2$, $\left(\hat{T}_2\right)^2$ etc., unlike the CISD method which can only include singles and doubles excitation contributions. Another advantage of this exponential ansatz is the property of size consistency[15]. It means that the sum of the CC energies of non-interacting fragments (each calculated separately) is equal to the energy of the supermolecule when all fragments are included in the calculations. CC methods give very accurate results for molecules at their equilibrium geometries[5]. CCSD(T) is often referred as the "gold standard" method of electronic structure theory. However, CC methods are computationally expensiver: CCSD scales as $O(N^6)$, CCSD(T) as $O(N^7)$, CCSDT as $O(N^8)$ and so on, where N is the number of basis functions.

CC analytic derivatives

Molecular properties like dipole moments, IR intensities, force constants etc., depend upon the gradients of the molecular energy with respect to external perturbations. In this section, a derivation of first order gradient expressions of the CC method is presented.

The gradient of the CC energy with respect to any external perturbation X is written as:

$$\frac{\partial E_{cc}}{\partial X} = \langle \Psi_o | \frac{\partial \bar{H}}{\partial X} | \Psi_o \rangle = \langle \Psi_o | \bar{H}^X + [\bar{H}, \frac{\partial \hat{T}}{\partial X}] | \Psi_o \rangle \tag{2.15}$$

where, $\bar{H}^X = e^{-\hat{T}} \frac{\partial \hat{H}}{\partial X} e^{\hat{T}}$ contains the derivatives of the basis functions, MO coefficients etc. Invoking the resolution of identity (RI),

$$1 = |\Psi_o\rangle\langle\Psi_o| + \sum_{ia} |\Psi_i^a\rangle\langle\Psi_i^a| + \frac{1}{4}\sum_{ijab} |\Psi_{ij}^{ab}\rangle\langle\Psi_{ij}^{ab}| + ... \tag{2.16}$$

equation (19) can be expressed as:

$$\frac{\partial E_{cc}}{\partial X} = \langle \Psi_o | \bar{H}^X | \Psi_o \rangle + \sum_{i.a.} \langle \Psi_o | \bar{H} | \Psi_{i.}^{a.} \rangle \langle \Psi_{i.}^{a.} | \frac{\partial \hat{T}}{\partial X} | \Psi_o \rangle. \tag{2.17}$$

The second term of the above equation involves calculating derivatives of amplitudes i.e. $\langle \Psi_i^a | \frac{\partial \hat{T}}{\partial X} | \Psi_o \rangle = \frac{\partial t_i^a}{\partial X}$, which can be very computationally expensive if calculated directly. As a result, we would like to recast the above equation in something which is computationally practical. We start with the CC amplitude equations, say singles equation and take its derivative with respect to X.

$$0 = \langle \Psi_i^a | \bar{H}^X + [\bar{H}, \frac{\partial \hat{T}}{\partial X}] | \Psi_o \rangle \tag{2.18}$$

Using RI as before, we can write the above equation in the folllowing form:

$$\sum_{j.b.}\langle\Psi_i^a|\bar{H}-E_{cc}|\Psi_{j.}^{b.}\rangle\langle\Psi_{j.}^{b.}|\frac{\partial\hat{T}}{\partial X}|\Psi_o\rangle=-\langle\Psi_i^a|\bar{H}^X|\Psi_o\rangle \tag{2.19}$$

or,

$$\langle\Psi_{j.}^{b.}|\frac{\partial\hat{T}}{\partial X}|\Psi_o\rangle=-\sum_{ia}\langle\Psi_{j.}^{b.}|(\bar{H}-E_{cc})^{-1}|\Psi_i^a\rangle\langle\Psi_i^a|\bar{H}^X|\Psi_o\rangle \tag{2.20}$$

The above equation was derived by considering the gradient of just the singles equation. Including the gradient of all the other amplitude equations and plugging the modified equation into the expression for the gradient of energy eq.(21), we obtain:

$$\frac{\partial E_{cc}}{\partial X}=\langle\Psi_o|\bar{H}^X|\Psi_o\rangle-\sum_{i.a.}\langle\Psi_o|\bar{H}|\Psi_{i.}^{a.}\rangle\sum_{j.b.}\langle\Psi_{i.}^{a.}|(\bar{H}-E_{cc})^{-1}|\Psi_{j.}^{b.}\rangle\langle\Psi_{j.}^{b.}|\bar{H}^X|\Psi_o\rangle \tag{2.21}$$

We define a perturbation independent Λ operator such that:

$$\langle\Psi_o|\Lambda|\Psi_{j.}^{b.}\rangle=-\sum_{i.a.}\langle\Psi_o|\bar{H}|\Psi_{i.}^{a.}\rangle\langle\Psi_{i.}^{a.}|(\bar{H}-E_{cc})^{-1}|\Psi_{j.}^{b.}\rangle. \tag{2.22}$$

This Λ operator can be seen as a de-excitation operator and can be written as:

$$\Lambda=\Lambda_1+\Lambda_2+\Lambda_3+... \tag{2.23}$$

where $\Lambda_1=\sum_{ia}\lambda_a^i\{a_i^\dagger a_a\}$ is the singles de-excitation operator, Λ_2 is the doubles de-excitation operator and so on. Using the lambda operator, the gradient expression gets simplified as:

$$\frac{\partial E_{cc}}{\partial X}=\langle\Psi_o|(1+\Lambda)\bar{H}^X|\Psi_o\rangle=\langle\Psi_o|(1+\Lambda)e^{-\hat{T}}\frac{\partial\hat{H}}{\partial X}|\Psi_{cc}\rangle \tag{2.24}$$

The governing equation for calculating the lambda amplitudes eq. (26) can be written in a more compact form:

$$\langle\Psi_o|(1+\Lambda)(\bar{H}-E_{cc})|\Psi_{i.}^{a.}\rangle=0 \tag{2.25}$$

Thus instead of taking the gradients of the non-linear T amplitude equations with respect to perturbations, we solve the linear perturbation-independent Λ equations for calculating the energy gradient.

Also, $\langle\Psi_o|(1+\Lambda)e^{-\hat{T}}$ is the CC left hand wavefunction and eq. (28) is a generalized Hellman-Feynman equation[22]. For full CC the left and right hand wavefunctions are Hermitian conjugates of each other, but this is not true for the truncated CC methods. This is because of the non-hermiticity of the $\bar{H}$ operator. However, for second order derivatives, we do need to calculate the first derivatives of either the T or Λ amplitudes with respect to a perturbation.

Coupled cluster linear response (CCLR)

CCLR method proposed by Koch and Jørgensen in 1990[32] is a recipe for accurate calculations of response properties like dynamic polarizabilities, optical rotations, etc. In this section, we will outline important steps for the derivations of both general and CCLR response functions and also talk about different gauge representations used for calculating the response functions.

The operator $V(t)$ which describes the interaction between the molecule and an external time-dependent field can be expressed in the frequency domain as:

$$V(t) = \int_{-\infty}^{\infty} d\omega \;\; V(\omega)e^{(-i\omega+\Gamma)t}, \tag{2.26}$$

The full Hamiltonian can then be written as: $H = H_o + V(t)$, where H_o is the time independent unperturbed Hamiltonian. Assuming that Ψ_o is an eigenstate of H_o and that the molecule is in state Ψ_o when the perturbation starts at $t = -\infty$, the $|\Psi_o\rangle$ state evolves in time as $|\Psi_o(t)\rangle$ according to the time-dependent Schrödinger equation.

$$i\frac{d}{dt}|\Psi_o(t)\rangle = (H_o + V^t)|\Psi_o(t)\rangle \tag{2.27}$$

Following the work of Olsen[47], the time dependent state $|\Psi_o(t)\rangle$ can be written as:

$$|\Psi_o(t)\rangle = |\bar{\Psi}_o\rangle e^{i\epsilon(t)} \tag{2.28}$$

where ϵ is a phase factor and the state $|\bar{\Psi}_o\rangle$ can be expressed as[32]:

$$|\bar{\Psi}_o\rangle = |\Psi_o\rangle + |\Psi_o\rangle^{(1)} + |\Psi_o\rangle^{(2)} + ... \tag{2.29}$$

where first order correction $|\Psi_o\rangle^{(1)}$ and others can be determined from the time dependent perturbation theory. For calculating any response property, the expectation value of the respective time independent operator is calculated in the presence of an external field. The response functions can be seen as the coefficients of terms which appear in different orders of perturbation in $V(t)$ in the expansion of the expectation value.[32]

$$\langle\Psi_o(t)|A|\Psi_o(t)\rangle = \langle\Psi_o|A|\Psi_o\rangle + \int_{-\infty}^{\infty} d\omega_1 \langle\langle A; V(\omega_1)\rangle\rangle_{\omega_1+i\Gamma} e^{(-i\omega_1+\Gamma)t} + ... \tag{2.30}$$

where we only considered the linear response function $\langle\langle A; V(\omega_1)\rangle\rangle$ and neglected the higher order terms. If the perturbation field is composed of a single frequency (ω_1) , the linear response function can be written as:

$$\langle\langle A; V(\omega_1)\rangle\rangle = \sum_k \{\frac{\langle\Psi_o|A|\Psi_k\rangle\langle\Psi_k|V(\omega_1)|\Psi_o\rangle}{\omega_1 - \omega_k + i\Gamma} - \frac{\langle\Psi_o|V(\omega_1)|\Psi_k\rangle\langle\Psi_k|A|\Psi_o\rangle}{\omega_1 + \omega_k + i\Gamma}\} \tag{2.31}$$

where ω_k is the excitation energy between the states Ψ_o and Ψ_k and the summation runs over all the solutions of the time independent Schrödinger equation Ψ_k. It can be seen from eq.(2) that $\mathbf{G}'(\omega)$ is nothing but the imaginary part of this response function if we take A as the dipole moment operator with V as a magnetic field. However, this approach is very computationally expensive for CC methods and we approximate the above linear response function using CCLR theory. Using the same approach as above, the right and left hand CC wavefunction evolve in time as[32]:

$$|\Psi_{cc}(t)\rangle = e^{\hat{T}(t)}|\Psi_o\rangle e^{i\epsilon(t)} \tag{2.32}$$

$$\langle\Lambda(t)| = \{\langle\Psi_o| + \sum_{i.a.} \lambda^{a.}_{i.}(t)\langle\Psi^{a.}_{i.}|e^{-\hat{T}(t)}\}e^{-i\epsilon(t)} \tag{2.33}$$

where $e^{\pm i\epsilon(t)}$ is a time dependent phase factor and we have time dependent T and $\lambda^{a.}_{i.}$ amplitudes. The governing equation for the time dependence of these amplitudes is the time-dependent Schrödinger equation.

$$i\frac{d}{dt}|\Psi_{cc}(t)\rangle = (H_o + V(t))|\Psi_{cc}(t)\rangle \tag{2.34}$$

$$\frac{d}{dt}\langle\Lambda(t)| = i\langle\Lambda(t)|(H_o + V(t)) \tag{2.35}$$

On multiplying eq. (38) by $e^{-\hat{T}(t)}$ on both sides and projecting it against $\langle\Psi^{a.}_{i.}|$, we obtain the expression for the time evolution of $t^{a.}_{i.}$ amplitudes.

$$\frac{dt^{a.}_{i.}}{dt} = -i\langle\Psi^{a.}_{i.}|e^{-\hat{T}(t)}(H_o + V(t))e^{\hat{T}(t)}|\Psi_o\rangle \tag{2.36}$$

On multiplying eq.(38) by $e^{i\epsilon(t)}$ and invoking the RI, the expression for time evolution of $\lambda^{b.}_{j.}$ amplitudes can be obtained:

$$\frac{d\lambda^{b.}_{j.}}{dt} = i\langle\tilde{\Lambda}(t)|[H_o + V(t), \{a^{\dagger}_b.a_j.\}]|\widetilde{\Psi}_{cc}(t)\rangle \tag{2.37}$$

where $\sim$ denotes the usual expressions without the phase factor $e^{\pm i\epsilon(t)}$. Expanding the $t_{i.}^{a.}$ amplitudes in orders of perturbation of V(t), the expressions for the different orders can be obtained using eq. (38). The first order derivative can be written as:

$$i\frac{d\, t_{i.}^{a.(1)}}{dt} = \langle \Psi_{i.}^{a.}|e^{-\hat{T}(0)}V(t)|\Psi_{cc}\rangle + \langle \Psi_{i.}^{a.}|e^{-\hat{T}(0)}[H_o, T^{(1)}]|\Psi_{cc}\rangle \tag{2.38}$$

The amplitude $t_{i.}^{a.}$ can be expressed in terms of its Fourier transform as:

$$t_{i.}^{a.(1)}(t) = \int_{-\infty}^{\infty} d\omega_1 X_{i.}^{a.(1)}(\omega_1 + i\Gamma)e^{(-i\omega_1+\Gamma)t} \tag{2.39}$$

where

$$X_{i.}^{a.(1)}(\omega_1 + i\Gamma) = \sum_{j.b.} \left\{(-A + (\omega_1 + i\Gamma)I)^{-1}\right\}_{i.a.}^{j.b.} \lambda_{j.}^{b.(1)}(\omega_1), \tag{2.40}$$

and

$$\lambda_{j.}^{b.(1)}(\omega_1) = \langle \Psi_{j.}^{b.}|e^{-\hat{T}(0)}V(\omega_1)|\Psi_{cc}\rangle. \tag{2.41}$$

A is the coupled cluster Jacobian matrix defined as:

$$A_{i.a.}^{j.b.} = \langle \Psi_{i.}^{a.}|e^{-\hat{T}}[H_o, \{a_b^\dagger.a_j.\}]|\Psi_{cc}\rangle \tag{2.42}$$

The above process is repeated with $\lambda_{b.}^{j.}$ amplitudes to obtain the derivative expressions and the Fourier transform Y.

$$\frac{d\, \lambda_{j.}^{b.(1)}}{dt} = i\langle\Lambda|([[H_o, \{a_b^\dagger.a_j.\}], T^{(1)}] + [V(t), \{a_b^\dagger.a_j.\}])|\Psi_{cc}\rangle + i\sum_{i.a.} \lambda_{i.}^{a.(1)} A_{i.a.}^{j.b.} \tag{2.43}$$

$$Y_{i.}^{a.(1)}(\omega_1+i\Gamma) = -\sum_{j.b.} \eta_{j.}^{b.(1)}(\omega_1) + \sum_{k.c.} F_{j.b.}^{k.c.} X_{k.}^{c.(1)}(\omega_1+i\Gamma)) \times \{(A + (\omega_1 + i\Gamma)I)^{-1}\}_{j.b.}^{i.a.} \tag{2.44}$$

where

$$\eta_{j.}^{b.(1)}(\omega_1) = \langle\Lambda|[V(\omega_1), \{a_b^\dagger.a_j.\}]|\Psi_{cc}\rangle, \tag{2.45}$$

and

$$F^{k.c.}_{j.b.} = \langle\Lambda|[[H_o, \{a^\dagger_b.a_j.\}], \{a^\dagger_c.a_k.\}]|\Psi_{cc}\rangle \tag{2.46}$$

The expectation value of any time dependent operator A in CC can be expanded in orders of perturbation.

$$\langle A\rangle = \langle\Lambda|A|\Psi_{cc}\rangle + \sum_{i.a.} \lambda^{a.(1)}_{i.}\langle\Psi^{a.}_{i.}|e^{-\hat{T}^{(0)}}A|\Psi_{cc}\rangle + \langle\Lambda|[A, T^{(1)}]|\Psi_{cc}\rangle + ... \tag{2.47}$$

Comparing this with equation (34), the CC linear response function can be determined.

$$\int_{-\infty}^{\infty} d\omega_1 \langle\langle A; V(\omega_1)\rangle\rangle_{\omega_1+i\Gamma} e^{(-i\omega_1+\Gamma)t} \equiv \sum_{i.a.} \lambda^{a.(1)}_{i.}\langle\Psi^{a.}_{i.}|e^{-\hat{T}^{(0)}}A|\Psi_{cc}\rangle + \langle\Lambda|[A, T^{(1)}]|\Psi_{cc}\rangle \tag{2.48}$$

In more general terms, the response function can be written as:

$$\langle\langle A; B\rangle\rangle_{\omega_1} = \sum_{i.a.}\langle\Lambda|[A, \{a^\dagger_a.a_i.\}]|\Psi_{cc}\rangle X^{a.}_{i.}(B, \omega_1) + \sum_{i.a.}\left\{\langle\Lambda|[B, \{a^\dagger_a.a_i.\}]|\Psi_{cc}\rangle + \sum_{k.c.} F^{k.c.}_{i.a.} X^{c.}_{k.}(B, \omega_1)\right\} X^{a.}_{i.}(A, - \tag{2.49}$$

where $X^{a.}_{i.}(B, \omega_1) = \sum_{j.b.}\left\{(-A + \omega_1 I)^{-1}\right\}^{j.b.}_{i.a.} B^{b.}_{j.}$,

and $B^{b.}_{j.} = \langle\Psi^{a.}_{i.}|e^{-\hat{T}^{(0)}}B|\Psi_{cc}\rangle$.

Thus for calculating the response functions, we need to solve two sets of linear equations for obtaining $X^{a.}_{i.}(B, \omega_1)$ and $X^{a.}_{i.}(A, -\omega_1)$. Thus, we can use this linear response formalism and can calculate the $\mathbf{G}'$ tensor using eq.(4) in which A is the dipole moment operator and B is the magnetic field. However, there can be different representations of an operator which are referred to as gauges. It is observed that in the truncated CCLR method if the length gauge representation of the dipole operator is used, i.e. $\mu \equiv r$ (in atomic units), the optical

rotation results are origin dependent. This problem is overcome in CCLR by using the velocity gauge representation where $\mu \equiv r \times p$. However, both these gauges are equivalent for exact wavefunctions. However, the velcity gauge calculated optical rotation does not decay to zero at the static limit, i.e. when the external field is zero, which is an unphysical result. To correct this problem, another representation called the modified velocity gauge (MVG) proposed by Pedersen [49] is used which shifts the values obtained by velocity gauge by its static limit.

2.2 Solvation Models

For the purpose of computational practicality, the QM solvation models aim to reduce the degrees of freedom of the solvent molecules without compromising the quality of description of the solvent-solute and the solvent-solvent interactions.

In this regard, the molecular mechanics (MM) based models, broadly known as QM/MM methods, usually represent the solvent molecules in the form of a classical potential by replacing them with point charges, polarizabilities etc.[] This potential polarizes the charge distribution of the solute which in turn creates a new potential or field because of which induced dipole moments appear in solvents (depending on the point polarizabilities), resulting in a new potential which again polarizes the solute and so on. Thus, the final one-electron solvent potential is attained in a self-consistent procedure and gets added to the solute's Hamiltonian for further response calculations. Fluctuating charge model(FQ)[], the drude

oscillator model[] and effective fragmentation potential (EFP)[] are some other popular examples of QM/MM methods.

Quantum continuum models like the polarizable continuum model (PCM)[] on the other hand place the solute in a cavity and replace the solvent molecules by a dielectric medium. The solute-solvent interactions are then captured by adding charges on the surface on the cavity (apparent surface charges) which are solved in a self-consistent manner as described above.

Mennucci et al. extended PCM to work with the linear response formalism of TD-DFT[41] and calculated optical rotations for chiral molecules in different solvents. They were able to obtain promising results

More recently, Cappelli implemented the QM/FQ/PCM approach for calculating optical rotations of methyloxirane

with molecular dynamics (MD) simulations

a series of snapshots from the MD is extracted, which constitute the actual model system on which the QM/FQ/PCM calculations of the desired properties are performed and then averaged out to obtain the final results. Actually, the computational cost of the procedure is mainly determined by the cost of the single QM/FQ/PCM calculation, which basically depends on the QM level and the kind of property (first, second, third derivative, etc.) to be calculated, together with the number of representative snapshots necessary to allow the

final results to converge to a sensible value.

FQ/PCM/MM has been combined by

In recent years, the ab inito methods mentioned above have been combined with various solvation based approaches[46, 45, 41, 68, 16] to calculate the optical rotation in solution. This review condiders some of the popular approaches that are being used and describes their working mechanisms and performances in detail. In the current/future work section of this review, some reduced scaling techniques are proposed with the aim of making these methods more efficient and computationally practical. Also, some of the essential, underlying coupled cluster and response theory used for optical rotation calculations are presented and discussed.

Chapter 3

Frozen Virtual Natural Orbitals for Coupled-Cluster Linear-Response Theory

3.1 Introduction

In the construction of many-body electronic wave functions, the scaling of a given method with the number of molecular orbitals (MOs) plays a pivotal role in the ultimate cost of the calculation. For many-body methods such as coupled cluster (CC),[59, 24, 13] which, in its canonical formulation, displays a higher-order polynomial dependence on the number of MOs, numerous mechanisms have been explored over the last half century for reducing

the size of the virtual-MO space. Among the earliest of these was Löwdin's[37] introduction in 1955 of the concept of "natural orbitals" (NOs) — orbitals for which the one-electron density matrix is diagonal. Löwdin demonstrated that NOs yield faster convergence of the configuration interaction (CI) wave function expansion than Hartree-Fock MOs. Some years later, Bender and Davidson[7] used natural orbitals in conjunction with CI (NO-CI) calculations to construct and analyze the most important configurations contributing to the correlated wave functions for a series of closed- and open-shell first-row diatomic hydrides. This work motivated Barr and Davidson a year later[4] to utilize only the virtual natural orbitals, obtained by diagonalization of the virtual-virtual block of the one-electron density matrix, for NO-CI calculations on the Ne atom.

The concept of pair natural orbitals (PNOs – originally called "pseudonatural orbitals") was developed by Edmiston and Krauss,[20] by Meyer[43], and by Ahlrichs and co-workers.[2] In the PNO approach, the virtual-virtual MO block of the one-electron density is constructed and diagonalized independently for each occupied MO pair, leading to separate non-orthogonal virtual spaces. Although this approach leads to rapid convergence of the correlation energy with respect to the size of the virtual space, it was little used following initial investigations until it was resurrected in recent years by Neese and co-workers with great success in the context of reduced-scaling electron correlation methods.[44, 53]

Following these pioneering efforts, NOs have been exploited in numerous applications to construct compact CI,[21, 61, 1] multiconfigurational self-consistent-field (MCSCF),[27] and CC wave functions.[62, 66, 67, 35, 18, 17] In many of these studies, the virtual-MO block

of the one-electron density is first obtained from a simpler model, such as second-order many-body perturbation theory (MBPT) calculation, and then diagonalized to yield the virtual-NO space. The space is then truncated based on an occupation-number-related criterion and fixed for the subsequent correlated-wave-function calculation. In addition, the final energy is commonly corrected using the second-order Møller-Plesset perturbation theory (MP2) correlation energy contributions arising from the external virtual space. These studies have indicated that, for energetics and related properties, even aggressive truncation of the virtual-NO space often has only a small impact on the resulting property as compared to full-space computations. For example, Landau *et al.*[35] found that, for NOs combined with the equation-of-motion coupled-cluster method for ionized states (EOM-IP-CC), reduction of the virtual space by up to 70% yielded truncation errors within ca. 1 kcal/mol for ionization energies of organic compounds and non-parallelity errors in potential surfaces of weakly bound complexes.

While the above studies have demonstrated clearly the usefulness of NOs for aggressively truncating the virtual space when computing correlation energies, more complex properties have yet to be considered. As shown in a number of recent reports,[34, 55, 56, 40, 23, 39] properties that are related to the linear- or higher-order response of the wave function to external electric and magnetic fields, for example, exhibit much greater sensitivity to the quality of the wave function than simple energetics. In particular, local correlation methods have been shown[34, 55, 56, 40, 39] to require significantly larger domains for properties such as polarizabilities than for ground-state energies. Furthermore, the many-body expansion

— which has yielded impressive convergence for energetics and dipole moments for clusters of weakly interacting molecules (such as a solute embedded in an explicit solvent) — converges erratically, at best, for spectroscopic response properties due to its strong basis-set dependence.[38] In order to account for this, the ability to reduce the dimensionality of the virtual space becomes paramount. Thus, the focus of the present work is on the extension of the NO approach to linear-response properties, especially the case of frequency-dependent dipole polarizabilities.

3.2 Theoretical Background

3.2.1 Frozen Virtual Natural Orbitals

The MP2 unrelaxed one-electron density matrix can be written in terms of spin orbitals as:

$$\gamma_{pq} = \langle \Psi^{(1)} | \{ a_p^\dagger a_q \} | \Psi^{(1)} \rangle, \tag{3.1}$$

where $|\Psi^{(1)}\rangle$ is the first order correction to the Hartree-Fock wave function,

$$|\Psi^{(1)}\rangle = \frac{1}{4} \sum_{ijab} t_{ij}^{ab} |\Phi_{ij}^{ab}\rangle \tag{3.2}$$

and

$$t_{ij}^{ab} = \frac{\langle ij||ab\rangle}{\epsilon_i + \epsilon_j - \epsilon_a - \epsilon_b}. \tag{3.3}$$

Here, $\langle ij||ab\rangle$ is an antisymmetrized two-electron integral in Dirac's notation and $.pdfilon_i, \epsilon_a ...$ refer to the Hartree-Fock molecular orbital energies. We use the indices $i, j, k, ...$ to indicate

occupied orbitals while $a, b, c, ...$ denote virtual orbitals. $|\Phi_{ij}^{ab}\rangle$ refers to a doubly-excited determinant where occupied orbitals i and j are replaced by virtuals a and b respectively. The brackets around the second-quantized operators in Eq. (3.1) indicate normal ordering with respect to the reference wave function.

In the MP2 based NO method, the virtual-virtual block of γ_{pq} is constructed,

$$\gamma_{ab} = \frac{1}{2} \sum_{ijc} t_{ij}^{ac} t_{ij}^{bc}, \tag{3.4}$$

and then diagonalized,

$$\boldsymbol{\gamma V} = \boldsymbol{nV}. \tag{3.5}$$

The eigenvectors, $\boldsymbol{V}$, are the virtual natural orbitals (NOs), and the eigenvalues, $\boldsymbol{n}$, are the associated occupation numbers. As noted earlier, the wave function amplitudes contain significantly greater sparsity when represented in the NO basis than the original canonical MO basis; orbitals with lower occupation numbers yield $\hat{T}_2$ amplitudes with smaller magnitudes and concomitantly smaller contributions to the correlation energy. Thus, orbitals with occupation numbers below a selected threshold can be removed without introduction of significant errors, leading to reduced computational cost. The Hartree-Fock virtual molecular orbitals and associated integrals are then transformed to this truncated NO basis, followed by semicanonicalization of the virtual-virtual block of the Fock matrix, for subsequent computations using higher-order correlation methods such as CC theory. In most cases, the final correlation energy in the truncated virtual space is corrected using the MP2 energy in the external (non-truncated) NO space to minimize the resulting errors, as described below.

3.2.2 Coupled Cluster Response Theory

Dynamic response functions representing higher-order properties such as polarizabilities and hyperpolarizabilities, optical activity tensors, magnetizabilities, etc. can be obtained by expanding the expectation value of an appropriate time-independent operator in perturbational orders with respect to a time-dependent external field. The CC form of response theory has been routinely used for many years for accurate calculations of such properties.[26] The CC linear response function for property operators $\boldsymbol{A}$ and $\boldsymbol{B}$, for example, can be written as

$$\langle\langle \boldsymbol{A}; \boldsymbol{B} \rangle\rangle_\omega = \frac{1}{2}\hat{C}^{\pm\omega}\hat{P}[A(-\omega), B(+\omega)] \left[\langle \Psi_0 | (1 + \hat{\Lambda}) \left([\bar{A}, \hat{X}^B_\omega] + \frac{1}{2}[[\bar{H}, \hat{X}^A_{-\omega}], \hat{X}^B_\omega] \right) | \Psi_0 \rangle \right] \tag{3.6}$$

where Ψ_0 is the reference wavefunction, $\hat{\Lambda}$ is a de-excitation operator used to parametrize the CC left hand wavefunction, ω is the frequency of the external field, $\hat{C}$ is a symmetrizer that simultaneously interchanges the sign of the field frequency and takes the complex conjugate of the expression, and $\hat{P}$ symmetrizes the expression with respect to the operators $\boldsymbol{A}$ and $\boldsymbol{B}$. Operators with an overbar have been similarity transformed with the ground state cluster operators, $\hat{T}$, e.g. $\bar{H} = e^{-\hat{T}}\hat{H}e^{\hat{T}}$. The first-order (right-hand) perturbed wave function is represented by $\hat{X}^B_\omega$, whose amplitudes can be obtained by solving a set of appropriate linear equations, e.g.,

$$\langle \Phi^{ab\cdots}_{ij\cdots} | (\bar{H} - \omega) | \hat{X}^B_\omega | \Psi_0 \rangle = -\langle \Phi^{ab\cdots}_{ij\cdots} | \bar{B} | \Psi_0 \rangle. \tag{3.7}$$

In the case of dynamic polarizabilities, for example, both $\boldsymbol{A}$ and $\boldsymbol{B}$ are cartesian components of the electric dipole operator, $\boldsymbol{\mu} = -\boldsymbol{r}$, and the isotropic polarizability α_ω is related to the

trace of the polarizability tensor such that Eq. (3.6) reduces to the following form (for real wavefunctions),

$$\alpha_\omega = \frac{1}{3}\mathrm{Tr}\left[\langle\Psi_0|(1+\hat{\Lambda})\left(\left[\bar{\mu},(\hat{X}^\mu_\omega+\hat{X}^\mu_{-\omega})\right]+\left[\left[\bar{H},\hat{X}^\mu_{-\omega}\right],\hat{X}^\mu_\omega\right]\right)|\Psi_0\rangle\right] \tag{3.8}$$

For dynamic polarizabilities computed using the coupled cluster singles and doubles (CCSD) method, for example, six sets of perturbed amplitudes, $\hat{X}_1(X_i^a)$ and $\hat{X}_2(X_{ij}^{ab})$, must be computed, one for each cartesian component of $\boldsymbol{\mu}$ at both positive and negative frequencies.

3.3 Computational Details

The primary molecular test cases of this work is hydrogen peroxide, H_2O_2, though additional tests are reported for related species such as (*P*)-dimethylallene and (*S*)-methyloxirane, as well as those same molecules interacting with one or more water molecules. All molecular structures were optimized using the B3LYP functional[6, 63, 36] in the aug-cc-pVDZ (aDZ) basis.[19, 29, 71] (Coordinates of all structures are provided in Tables S1-S5 of the Supporting Information.) Frequency-dependent polarizabilities were computed at the coupled cluster singles and doubles (CCSD) level of theory[51] using a linear-response formulation.[10] While the aDZ basis set was used for most test calculations, the larger aug-cc-pVTZ (aTZ) and aug-cc-pVQZ (aQZ) basis sets were also employed for selected analyses.[29] All orbitals were active in the correlated models utilized here, and all coupled-cluster calculations were carried out using the PSI4 open-source quantum chemistry package.[69] In all calculations in which virtual orbitals are truncated, the same orbital space is used in the solution of the

unperturbed and perturbed amplitudes equations, just as is required for locally correlated property calculations.[12] We note that the size-extensivity of the polarizability is unaffected by the truncation of the virtual space.

3.4 Results and Discussion

It is well known that deletion of higher-energy canonical Hartree-Fock MOs (CMOs) typically leads to significant errors in the recovery of electron correlation energies, whereas, by design, the truncation of virtual NOs with low occupation numbers results in little loss of accuracy.[35, 66, 67] For example, Fig. 3.1 plots the error in the CCSD correlation energy

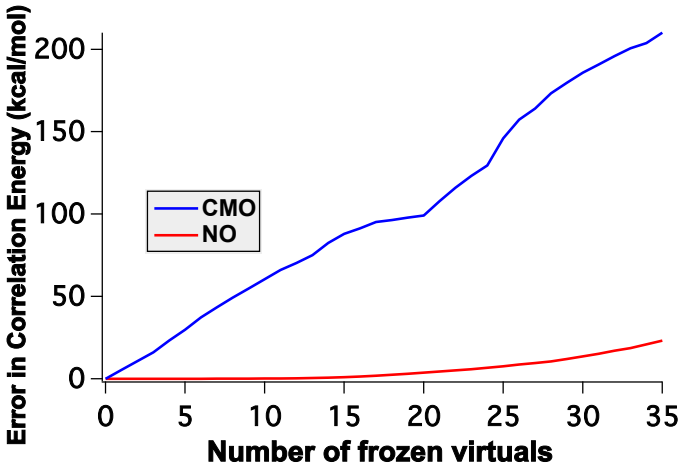

Figure 3.1: Error in the CCSD energy of H_2O_2 in kcal/mol as a function of the number of frozen virtual orbitals in both CMO and NO bases.

of H_2O_2 in the aDZ basis as a function of the number of frozen virtual CMOs (removed starting from the highest energy orbitals) or NOs (starting from the lowest occupation numbers). Clearly the correlation energy is very sensitive towards the removal of CMOs, with the error increasing by more than 4 kcal/mol after the deletion of even one virtual orbital. On the other hand, removal of low occupation-number NOs introduces errors of only ca. 2.5 kcal/mol even when up to 33% of the virtual space (18 of 55 orbitals) is truncated. The errors in the NO basis can be further minimized by employing an MP2 energy correction,

$$E_{\text{corr}}^{\text{MP2}} = \frac{1}{4}\sum_{ij}\sum_{ab\in\text{ext}} \frac{|\langle ij||ab\rangle|^2}{.pdfilon_i + \epsilon_j - \epsilon_a - \epsilon_b}. \tag{3.9}$$

where the summation over virtual orbitals is limited to NOs in the external, truncated space. Fig. 3.2 plots the error in the CCSD correlation energy for the same system as above in the

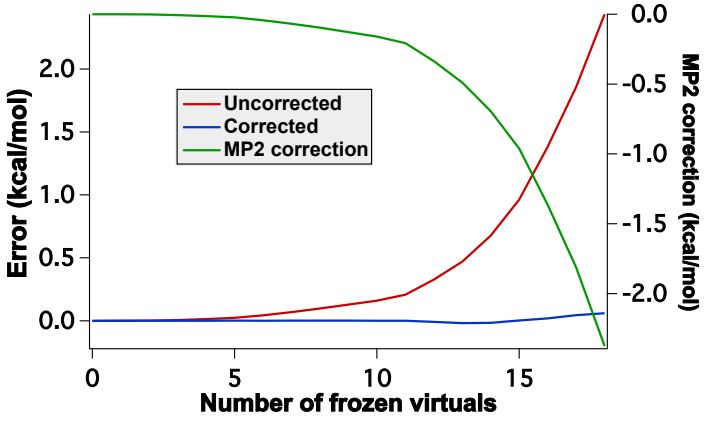

Figure 3.2: Error in CCSD energy of H_2O_2 in the NO bases, with and without MP2 corrections and MP2 correction as a function of the number of frozen virtual orbitals.

NO basis, with and without this correction (left-hand vertical axis), as well as the correction itself (right-hand axis). After employing the correction, the error in the correlation energy falls to less than 0.1 kcal/mol when 1/3 of the virtual space is eliminated. Similar results are obtained for aTZ and aQZ basis sets, where the truncation errors are less than 1 kcal/mol even after the removal of 50% of the virtual space. We note that the MP2 energy correction is significant (on the order of mE_h or several kcal/mol) even for small compounds such as H_2O_2. The correction scales linearly with the number of electrons and thus is a critical component for the success of the frozen virtual NO approach for larger molecules.

3.4.1 Frozen Virtual Orbitals and Response Properties

What is the impact of freezing virtual orbitals — whether CMO or NO — on higher-order properties? Fig. 3.3 plots errors in dynamic polarizabilites (computed at a wavelength of 589 nm) as a function of the number of virtual orbitals deleted at the CCSD/aDZ level of theory for the same H_2O_2 test case as above. Comparison to Fig. 3.1 reveals precisely the opposite behavior for polarizabilities as for correlation energies, *viz.*, truncation of the CMO virtual space induces much smaller errors than does that of the NO virtual space. For the latter, errors increase approximately linearly with the number of frozen virtual NOs. On the other hand, for the CMO basis, the error increases slowly to a maximum of 1.9% when 13 virtual orbitals are removed and then decreases to only -0.3% when as many as 27 orbitals (ca. 50% of the virtual space) are frozen. This trend is not unique to H_2O_2 or the aDZ basis set. As shown in Fig. S1 of the Supporting Information, the same behavior is observed

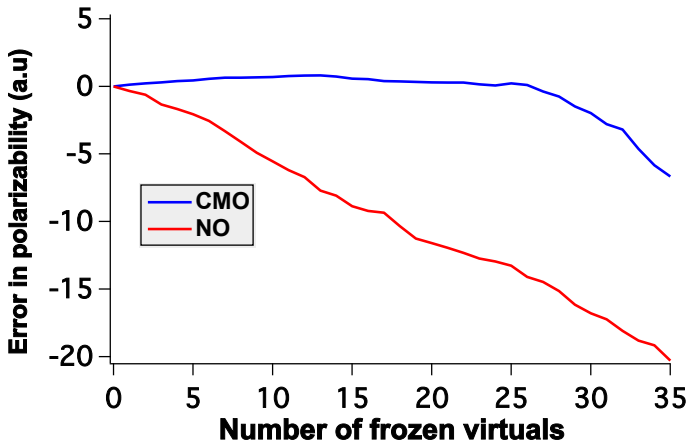

Figure 3.3: Errors in the CCSD/aDZ dynamic polarizability (589 nm) of H_2O_2 in in both CMO and NO bases as a function of number of virtual orbitals removed .

for other molecules such as dimethylallene, methyloxirane, and such compounds interacting with explicit solvent molecules. In addition, Figs. S2 and S3 report the same trends for H_2O_2 with the larger aTZ and aQZ basis sets.

What is the source of this unexpected behavior? It is well known that diffuse basis sets are essential for the accurate descriptions of a variety of response properties, such as dipole polarizabilities.[71] Fig. 3.4 plots the spatial extent — $\langle r^2 \rangle$ — for each virtual CMO or NO in the same ordering as they are deleted in Fig. 3.3. The Figure clearly shows that the earliest NOs to be removed (the ones with the lowest occupation numbers) are the most diffuse, *i.e.*, they should contribute substantially to the description of the dynamic polarizability. On the other hand, the first CMOs to be frozen (those with the highest orbital energies) are also the

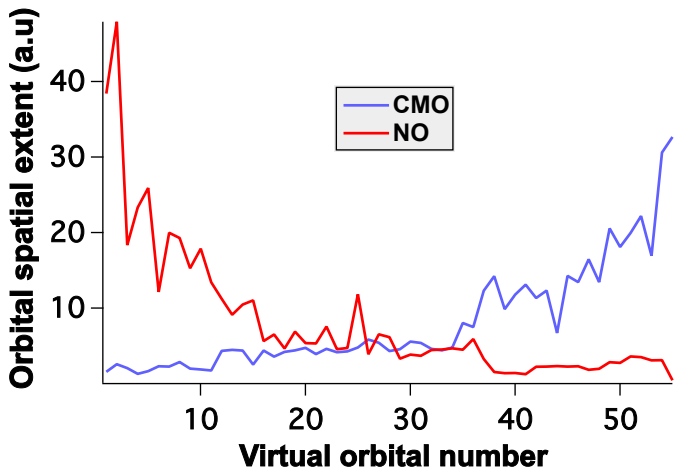

Figure 3.4: Spatial extent ($\langle r^2 \rangle$) of virtual orbitals of H_2O_2 in both CMO and NO bases. Orbitals are ordered left-to-right by decreasing energy (CMOs) or increasing occupation number (NOs).

most compact and thus contribute the least to this property. Given that highly diffuse basis functions typically contribute primarily to CMOs with low orbital energies — often below that of what is normally considered the true anti-bonding "LUMO" — the latter result is not surprising; these diffuse CMOs appear to the far right of Fig. 3.4 and are thus never deleted, leading to the good behavior of the CMO truncation in Fig. 3.3. These same diffuse basis functions, however, contribute little to the description of dynamical correlation effects, and thus exhibit very low occupation numbers upon transformation to the NO virtual space. Thus, they are truncated first in the NO basis, yielding the large errors in the polarizability depicted in Fig. 3.3.

The above observations suggest that, for computing response properties such as dynamic

polarizabilities, an alternative approach to truncation of the virtual space is to order the orbitals by increasing values of $\langle r^2 \rangle$ rather than by decreasing orbital energies (as is done for CMOs) or increasing occupation numbers (for NOs). Fig. 3.5 plots errors in the CCSD/aDZ

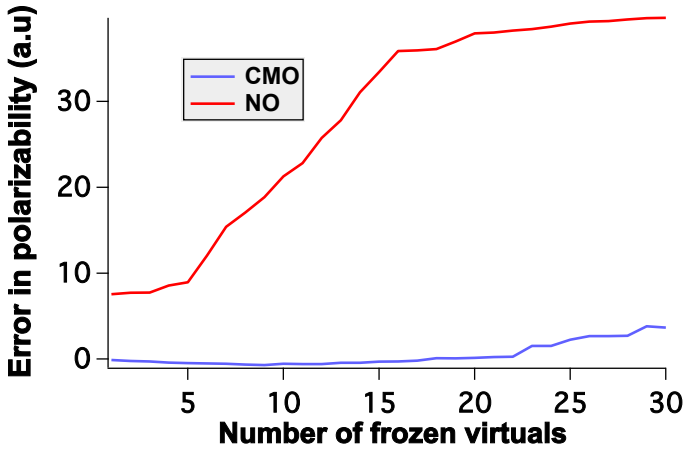

Figure 3.5: Spatial extent ($\langle r^2 \rangle$) of virtual orbitals of H_2O_2 in both CMO and NO bases. Orbitals are ordered left-to-right by decreasing energy (CMOs) or increasing occupation number (NOs).

dynamic polarizability of H_2O_2 as the virtual CMOs or NOs are removed in order of increasing spatial extent. While the errors are comparable to that observed in Fig. 3.3 for the CMO truncation, the behavior associated with removal of virtual NOs is significantly different. First, the polarizability errors exhibit two plateaus: one associated with diffuse NOs 2-5 and another with NOs 16-30, and removal of these NOs has little impact on the observed error. However, deletion of the virtual NO with the *smallest* spatial extent unexpectedly leads to a large initial error (ca. 7.5 a.u.), followed later by a linearly increasing error as virtual NOs

6-15 are removed. Clearly, spatial extent is not the only criterion by which we may predict the importance of a given virtual NO to the polarizability.

Another possible source of error is the lack of orbital response in the chosen formulation of the coupled cluster linear response function.[31] In the infinite-lifetime approximation, frequency-dependent properties such as dipole polarizabilities exhibit first-order poles at the excitation frequencies. In the coupled cluster formulation described above, the orbital response to the external field is typically neglected so that these poles correspond solely to the response for the correlated wave function, and additional, spurious poles arising due to the Hartree-Fock reference determinant will not appear. (This approximation is typically justified based on the fact that much of the orbital-response effects are accounted for by the singles amplitudes.[11]) In order to test whether the orbital relaxation significantly impacts the behavior of the computed polarizability as the virtual space is reduced, we have computed *static* ($\omega = 0.0$) polarizabilities using finite-differences (with a a central-difference formula with a differential field strength of 0.001 a.u.) The errors in the CCSD/aDZ static polarizability of H_2O_2 for both CMO and NO virtual spaces are reported in Fig. 3.6. Interestingly, with orbital relaxation included, the truncation of the NO space now becomes better behaved than the CMO space over a large domain of orbitals removed. Unfortunately, we cannot take advantage of this improvement in conjunction with Hartree-Fock orbitals without corrupting the pole structure of the response function. A Brueckner or orbital-optimized approach may prove superior in this regard, though further investigation is warranted.[31, 48]

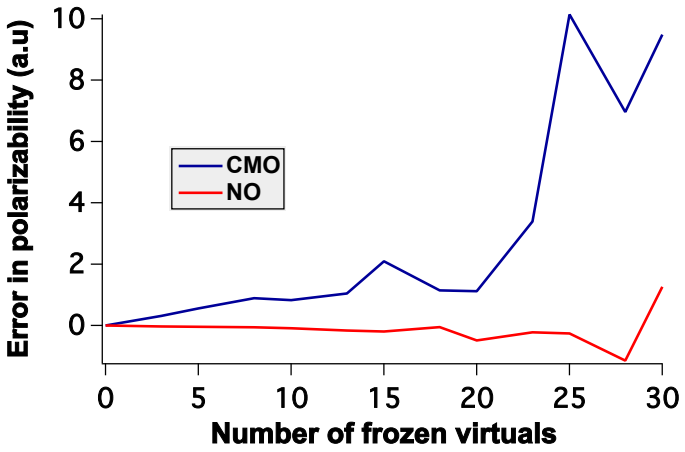

Figure 3.6: Errors in the CCSD/aDZ static polarizability (including orbital relaxation effects) of H_2O_2 in in both CMO and NO bases as a function of number of virtual orbitals removed.

3.4.2 Wave Function Truncation in the Virtual-Orbital Space

For additional insight into the above observations, we examine errors arising in dynamic polarizabilities as a function of truncation of specific wavefunction parameters in either the CMO or NO basis. Fig. 3.7 plots the errors in CCSD/aDZ dynamic polarizabilities of H_2O_2 as a result of truncations of the unperturbed ground-state cluster amplitudes $\hat{T}$ and $\hat{\Lambda}$, as well as perturbed amplitudes, $\hat{X}^{\mu}_{\omega}$, represented in the CMO basis. Note that, in this analysis, only the specified amplitudes associated with the selected CMOs are forced to zero; the CMOs remain active for all other wave function components. From the Figure, it can be clearly seen that removing $\hat{T}_1$ alone does not introduce any significant error in the polarizability, whereas truncating $\hat{T}_2$ amplitudes results in substantial positive errors which increase almost linearly

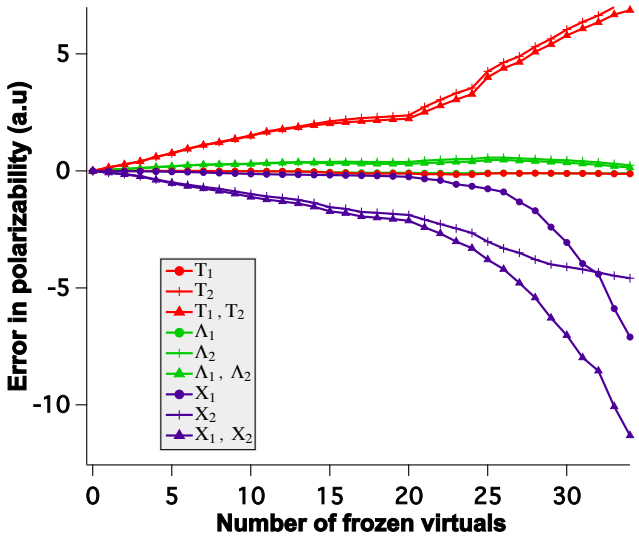

Figure 3.7: Errors introduced in CCSD/aDZ polarizabilities of H_2O_2 in the virtual CMO bases by the truncation of different classes of wave function amplitudes.

with the number of virtual CMOs. (Not surprisingly, freezing both $\hat{T}_1$ and $\hat{T}_2$ amplitudes together have essentially the same effect as freezing $\hat{T}_2$ amplitudes alone.) Alternatively, for the left-hand wave function, removing $\hat{\Lambda}_1$ and $\hat{\Lambda}_2$ amplitudes either separately or pairwise seem to have negligible impact. In the case of the perturbed amplitudes, only small (negative) errors are introduced even after freezing all $\hat{X}_1$ amplitudes involving almost 23 virtual CMOs, but the error then rises sharply with further truncation. On the other hand, the negative errors due to truncation of $\hat{X}_2$ amplitudes are significant from the beginning and increase almost linearly. Thus the error due to removal of both $\hat{X}_1$ and $\hat{X}_2$ amplitudes belonging to the first 23 CMOs is due to elimination of $\hat{X}_2$ amplitudes alone, whereas beyond that limit,

the total error corresponds to the sum of errors from $\hat{X}_1$ and $\hat{X}_2$ truncation.

A key observation is that, within the domain of the first 23 virtual CMOs, the positive errors introduced by truncation of $\hat{T}_2$ is cancelled almost exactly by the negative errors arising from the truncation of $\hat{X}_2$. This is further illustrated in Fig. **??**, which plots on a narrow range the

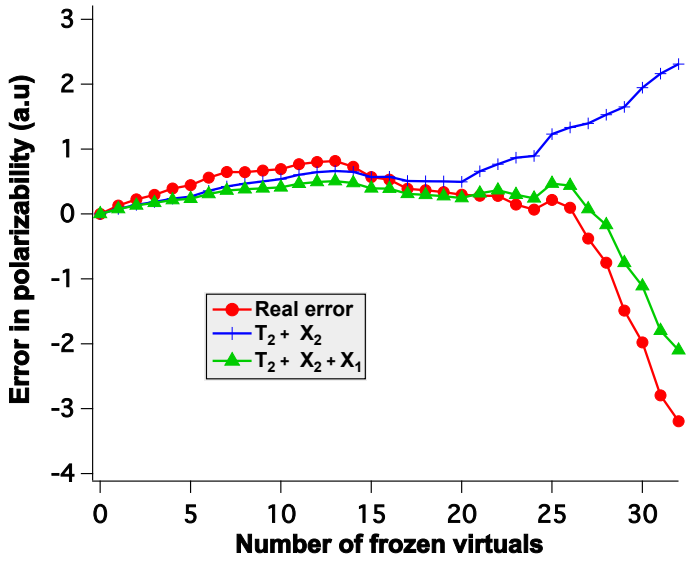

Figure 3.8: Errors introduced in CCSD/aDZ polarizabilities of H_2O_2 in the virtual CMO bases by the truncation of specific classes of wave function amplitudes as compared to the total errors obtained by freezing of virtual CMOs.

errors in the polarizability associated with truncating specific classes of $\hat{T}_2$ and $\hat{X}_2$ amplitudes against the total errors obtained by freezing CMOs entirely (for all amplitudes). Outside of this domain, errors associated with neglect of $\hat{X}_1$ amplitudes become dominant, leading to

the accumulation of negative total errors observed in Fig. 3.3. Thus, the apparently robust performance of the truncation of the virtual CMO space arises, in fact, from offsetting errors. Similarly to the above analysis for the virtual CMO space, Fig. 3.9 reports errors in the

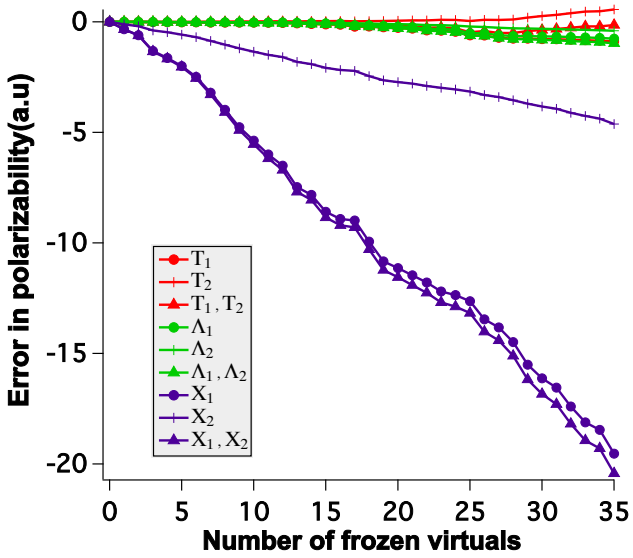

Figure 3.9: Errors introduced in CCSD/aDZ polarizabilities of H_2O_2 in the virtual NO bases by the truncation of different classes of wave function amplitudes.

CCSD/aDZ polarizability of H_2O_2 introduced by the neglect of various classes of wave function amplitudes associated with selected virtual NOs. We observe first that, unlike the CMO case, neglecting $\hat{T}_2$ amplitudes associated with particular virtual NOs has no significant effect on the error. This behavior is expected, because the $\hat{T}_2$ amplitudes are, by construction, sparse in the virtual NO basis such that orbitals with low occupation numbers are associated

with $\hat{T}_2$ amplitudes of smaller magnitude. Furthermore, just as in the CMO case, the removal of $\hat{T}_1$, $\hat{\Lambda}_1$ and $\hat{\Lambda}_2$ amplitudes introduces only small errors, while the removal of selected $\hat{X}_2$ amplitudes based on NOs yields significant negative errors that increase linearly with the number of virtual NOs truncated.

However, unlike the virtual CMO case, neglecting $\hat{X}_1$ amplitudes corresponding to specific virtual NOs introduces large negative errors in the polarizability even from the first NO removed, and the total error obtained by truncating both $\hat{X}_1$ and $\hat{X}_2$ amplitudes is almost the same as the error due to truncation of the $\hat{X}_1$ amplitudes alone. Indeed, the greatest contribution ($> 90\%$) to the total polarizability errors arises from the perturbed singles amplitudes.

The significance of the $\hat{X}_1$ amplitudes is evident upon analysis of their leading-order contribution to the polarizability [cf. Eq. (3.8)],

$$\alpha_\omega \leftarrow \frac{1}{3}\sum_{ia}\sum_{x}\mu_{ia}^{x}(X_{ia}^{x}(\omega)+X_{ia}^{x}(-\omega)), \tag{3.10}$$

where μ_{ia}^{x} is an element of the occupied-virtual block of the Cartesian component, x, of the electric-dipole moment integral matrix, and the inner sum runs over all such components. The singles themselves are obtained from the corresponding form of Eq. (3.7),

$$\langle\Psi_i^a|X_\omega^\mu|\Psi_0\rangle = -\sum_{\nu}\langle\Psi_i^a|(\bar{H}-\omega)^{-1}|\nu\rangle\langle\nu|\bar{\mu}|\Psi_0\rangle, \quad \nu\in\{\Psi_j^b,\Psi_{jk}^{cd}\}, \tag{3.11}$$

where $\bar{\mu}$ is the similarity transformed electric-dipole operator,

$$\bar{\mu} = \hat{\mu} + \left[\hat{\mu},\hat{T}\right] + \frac{1}{2}\left[\left[\hat{\mu},\hat{T}\right],\hat{T}\right]. \tag{3.12}$$

The corresponding leading-order contribution to the $\hat{X}_1$ amplitudes themselves is

$$X_{ia}^{\mu}(\omega) \leftarrow \frac{\mu_{ia}}{\overline{H}_{ii} - \overline{H}_{aa} + \omega}, \tag{3.13}$$

where the largest contribution to the diagonal elements of the similarity transformed Hamiltonian, $\bar{H}$, arises from the orbital energies (more precisely, the diagonal Fock matrix elements expressed in the CMO or NO basis), which are plotted in Fig. 3.10. While the values for the

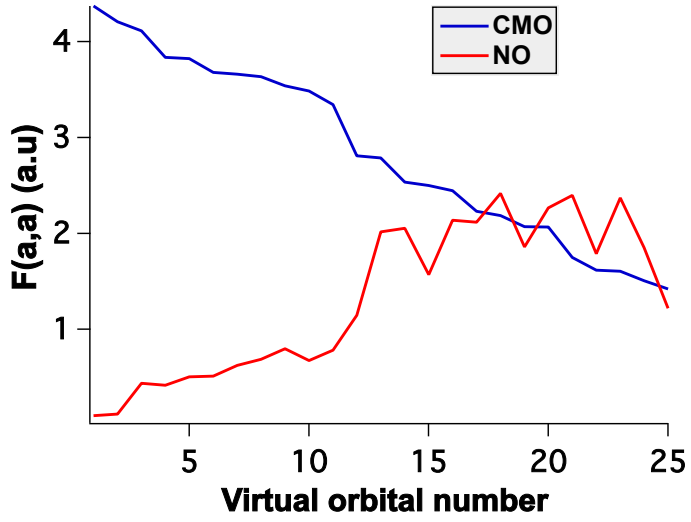

Figure 3.10: Virtual diagonal elements (a.u.) of the Fock matrix in the CMO and NO bases.

virtual CMOs decrease steadily, their NO counterparts actually *increase* and display greater oscillation. Clearly, the diagonal elements of the fock matrix for virtual NOs are significantly smaller in magnitude than the corresponding CMOs, which concomitantly increases the values of the $\hat{X}_1$ amplitudes associated with such NOs. This effect can be seen in Fig. 3.11 which plots the sum of the absolute values of $\hat{X}_1$ amplitudes for a given virtual orbital, i.e.

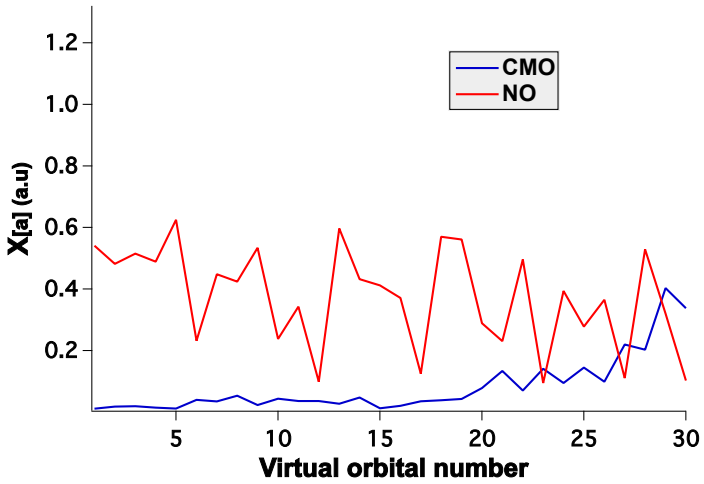

Figure 3.11: Sum of the absolute values of $\hat{X}_1$ amplitudes for a given virtual, $\sum_i |X_i^a|$, for perturbation μ_x and frequency 589 nm, plotted for each virtual NO or CMO.

$\sum_i |X_i^a|$, for both virtual CMOs and NOs. Thus, the sparsity of the $\hat{X}_1$ amplitudes present in the CMO basis is almost completely lost in the NO basis, which leads to the large errors in dynamic polarizabilities due to the truncation of $\hat{X}_1$ amplitudes in the NO basis observed earlier.

Furthermore, the dependence of the $\hat{X}_1$ amplitudes on both $\hat{T}_2$ and $\hat{X}_2$ plays a significant role in the overall *sign* of the polarizability error. This point is clearly illustrated in Fig. 3.12, which plots the 2-norm of the $\hat{X}_1$ vector as $\hat{T}_2$ or $\hat{X}_2$ amplitudes associated with a given virtual CMO is neglected (in the same manner as used in Figs. 3.7 and 3.8). As the $\hat{T}_2$ amplitudes associated with a given virtual orbital are removed, the norm of the $\hat{X}_1$ vector

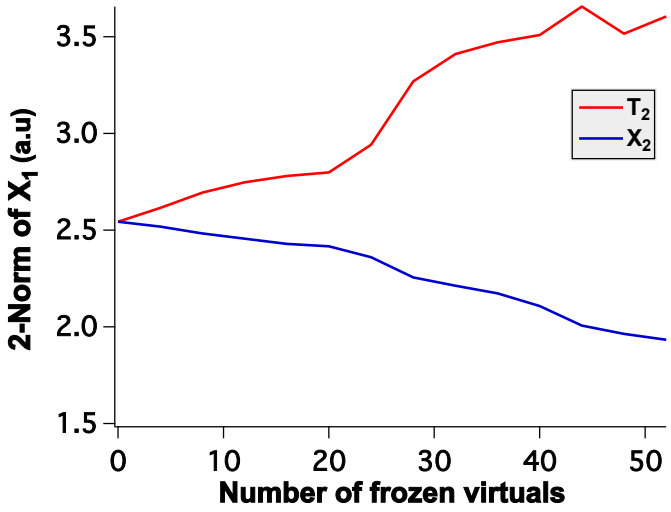

Figure 3.12: The 2-norm of the $\hat{X}_1$ amplitude vector in the CMO bases as a function of the truncation of classes of unperturbed $\hat{T}_2$ and perturbed $\hat{X}_2$ amplitudes.

increases, leading to the positive errors in the polarizability observed in Fig. 3.7. On the other hand, removal of $\hat{X}_2$ amplitudes leads to a decrease in the norm of the $\hat{X}_1$ vector and the negative errors in the polarizability appearing in Fig. 3.7.

3.4.3 External-Space Corrections

As noted earlier, a key aspect of the strong performance of virtual NOs for correlation energies is the use of MP2-based corrections for the contributions of the truncated or "external" virtual space, as given in Eq. (3.9). When considering a similar correction for properties, however, we have explored three options: time-dependent Hartree-Fock (TDHF) and both

static and dynamic CC2[11] corrections. In each case, we have used the same MP2-based virtual NO space and computed the correction as the difference between the full-virtual space polarizability and the truncated virtual-NO polarizability, with the CCSD/aDZ results for polarizabilties of H_2O_2 shown in Fig. 3.13. The CC2-based corrections recover nearly all of

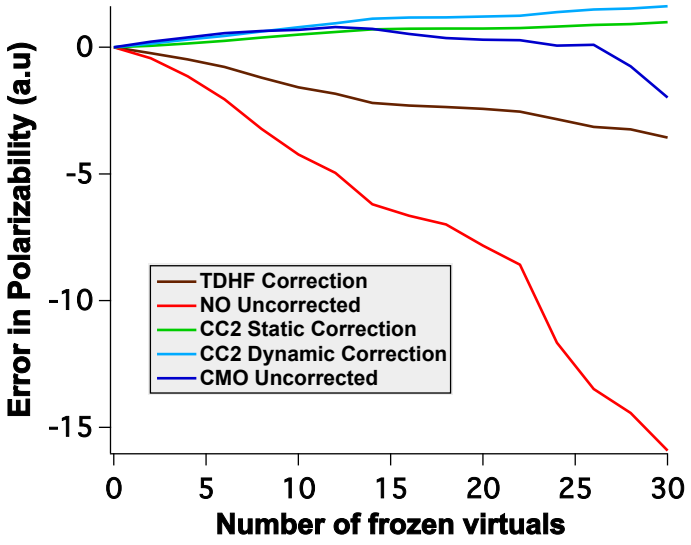

Figure 3.13: Correction schemes for the external truncated NO space for the CCSD/aDZ polarizabilities of H_2O_2.

the error associated with the uncorrected virtual NO space across a wide range of truncation, with the static correction actually yielding slightly smaller errors than its dynamic counterpart. The less expensive TDHF corrections offer significant improvement over the original virtual NO results, and recover most (ca. 85%) of the error until about 40% (21 orbitals) of the virtual space has been deleted, but it clearly produces overall larger errors than the

correlated methods. In addition, the TDHF corrections are potentially problematic because the pole structure of the polarizability naturally follows that of the underlying Hartree-Fock perturbed orbitals rather than that of the correlated wave functions,[52, 25, 3] a criticism that would also hold for purely MP2-based corrections. On the other hand, the CC2-based corrections are significantly more expensive than TDHF, in part because of their iterative nature and the need to transform two-electron integrals involving three virtual orbitals (with the latter criticism again holding for an MP2-based correction).

3.4.4 Perturbed Natural Orbitals

Given that the purpose of the NOs is to "focus" the important components of the basis for the description of electron correlation effects into a compact space, without consideration of the importance of the basis set for other properties, an alternative approach might be to build a virtual space that explicitly takes such properties into account, such as the inclusion of the perturbed one-electron density in the definition of the space. Instead of diagonalizing the ground-state MP2 density, we diagonalize its gradient with respect to the external electric field, thereby incorporating the effects of the external perturbations. The resulting "occupation numbers" obtained thus carry information about orbital occupancies in the perturbed states. The x^{th} Cartesian component of the perturbed density matrix can be written in terms of spin orbitals as

$$\gamma^x_{ab} = \frac{1}{2}\sum_{ijc} P_+(a,b)\left[\frac{t^{bc}_{ij}}{D^{ac}_{ij}}\left(P_-(a,c)\sum_d t^{ad}_{ij}\mu^x_{cd} - P_-(i,j)\sum_m t^{ac}_{im}\mu^x_{mj}\right)\right] \tag{3.14}$$

where P_+ and P_- are symmetric and anti-symmetric permutation operators, respectively, and the orbital-energy denominator $D_{ij}^{ac} = \epsilon_i + \epsilon_j - \epsilon_a - \epsilon_c$. (For computational convenience, orbital relaxation terms have been neglected.) To obtain the perturbed NOs and their corresponding eigenvalues, we take an average of the three cartesian components of the density and diagonalize the result. The eigenvalues consist of both positive and negative values as the perturbed density matrix is not positive definite, and thus we truncate the orbitals based on the absolute values of these eigenvalues. Fig. 3.14 compares the performance of

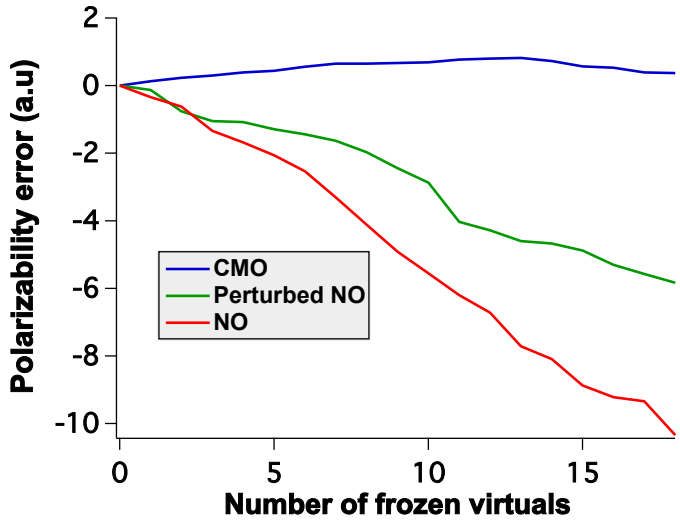

Figure 3.14: Errors introduced in CCSD/aDZ polarizabilities of H_2O_2 in the virtual CMO and NO bases, as well as the perturbed virtual NO basis as a function of number of virtual orbitals removed.

these perturbed NOs with that of the CMOs and NOs, where the error in the CCSD/aDZ dynamic polarizability of H_2O_2 is plotted as a function of the number of virtual orbitals

removed. While the perturbed NOs lower the truncation errors associated with conventional NOs, they still introduce significantly higher errors than the corresponding CMOs. The reason for this underperformance is related to the definition of the perturbed density, which naturally bears strong similarity to its unperturbed counterpart [cf. Eqs. (3.4) and (3.14).] As a result, similar sparsity and orbital energy issues illustrated in Figs. 3.10 and 3.11 arise for the perturbed density just as for the original NOs, indicating that such an approach does not resolve the problem.

3.4.5 The Dipole-Amplitude Criterion

The above results demonstrate that the CMO basis provides the best performance among the various virtual spaces considered here, albeit based on cancellation of errors, but what criterion should be used to determine the truncation level that provides optimal balance between computational cost (most compact virtual space) and accuracy? The CMO orbital energies are one possibility, but they have no direct connection to the properties in question. Another alternative is the "dipole amplitude", d_a, which is defined for each virtual CMO as

$$d_a \equiv \sum_x \sum_i \frac{(\mu_{ia}^x)^2}{.pdfilon_i - \epsilon_a}. \tag{3.15}$$

This expression, which is trivially computed post-Hartree-Fock, is based on Eqs. (3.10) and (3.13), using the fact that the leading contributions to the diagonal elements of the similarty-transformed Hamiltonian are the orbital energies. As we are constructing a phenomenological truncation criterion, we have chosen to neglect the dependence on the field

frequency. Fig. 3.15 plots the values of the dipole amplitude for each CMO, as well as the

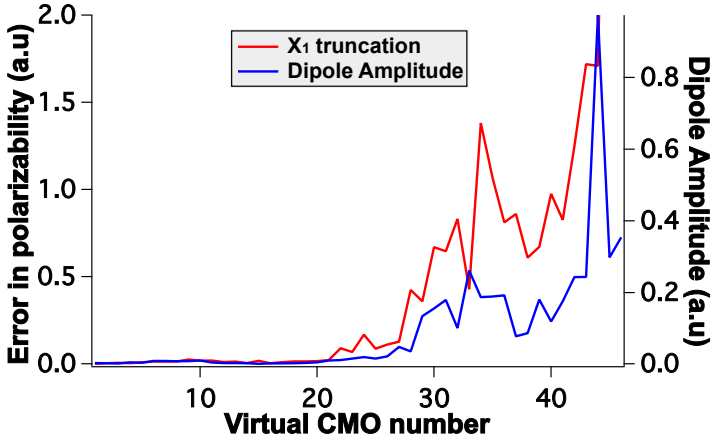

Figure 3.15: Absolute errors introduced in CCSD/aDZ polarizabilities of H_2O_2 due to truncation of $\hat{X}_1$ amplitudes and dipole amplitudes plotted as a function of different virtual CMOs.

corresponding error in the CCSD/aDZ dipole-polarizability of H_2O_2 introduced by deleting the $\hat{X}_1$ amplitude associated with a given virtual CMO. There is a clear correlation between the two functions, and one can see that as both the error due to truncation of $\hat{X}_1$ and the value of the dipole length increase sharply once we reach CMOs 27-28 — ca. 50% of the virtual space for this test case. Accordingly, one should stop the truncation of the virtual CMO space once the dipole length values start rising sharply. While the optimal choice of such a threshold will be addressed systematically in subsequent work, our preliminary analyses using H_2O_2, methyloxirane, dimethylallene, and related compounds suggest a cutoff of ca. 3-3.5% yields minimal errors in the polarizability.

3.5 Conclusions

On the basis of the above findings, we conclude that, in the absence of orbital relaxation, virtual NOs are not suited for higher-order property calculations such as dynamic polarizabilities, and that the occupation number is not an acceptable criterion for estimating the importance of a virtual orbital for such calculations. Although the use of external space corrections based on CC2 polarizabilities reduces the observed truncation errors, they are too relatively costly to be practical for large molecular systems. Furthermore, the use of perturbed virtual NOs offers only slight improvement as compared to unperturbed virtual NOs. CMOs, on the other hand, provide a much more stable mechanism for reducing the size of the virtual space — with truncation of up to 50% of the orbitals yielding shifts of less than 2% as compared to full-space calculation – but the source of their success lies in a significant cancellation of errors. Although further systematic studies are needed, the dipole amplitude appears to provide a useful threshold for an *a priori* truncation of the CMO virtual space.

3.6 Acknowledgements

This research was supported by a grant (CHE-1465149) from the U.S. National Science Foundation. The authors acknowledge Advanced Research Computing at Virginia Tech for providing computational resources and technical support that have contributed to the results reported within this paper.

Chapter 4

Perturbed Natural Orbitals for Coupled-Cluster Linear-Response Theory

4.1 Introduction

One of the central problems limiting the application of accurate *ab initio* methods like coupled-cluster (CC) theory to large molecular systems is their high computational costs, i.e., their computing and storage requirements exhibit polynomial scaling with the size of the system or equivalently with the number of one electron basis functions used in these calculations. Specifically, the size of the virtual space is of greater concern since they usually

far outnumber the occupied orbitals. Furthermore, the canonical virtual orbitals obtained from the Hartree-Fock (HF) procedure are non-local in nature and hence the convergence of a determinantal expansion involving these orbitals is quite slow. However, Löwdin []showed that using "natural orbitals" (NOs) instead of canonical HF orbitals can significantly accelerate the convergence of the configuration interaction (CI) wavefunction expansion. The NOs are the eigenvectors of the 1 electron reduced density matrix (1-RDM) associated with a wavefunction. The corresponding eigenvalues are commonly referred to as "occupation numbers". Since Löwdin's pioneering work, NOs have found a lot of applications especially in techniques aimed at obtaining a compact representation of the virtual space for correlated calculations.[] Please refer to ref. [35] for an excellent overview on this subject. Within the context of the CC theory, the frozen virtual NO (FVNO) scheme where the NOs are usually obtained from the 1-RDM of a less expensive correlated method such as second-order Möller-Plesset (MP2) theory and the virtual space for subsequent CC calculations is truncated based on the orbitals' occupation numbers has been used quite successfully to calculate correlation energies, ionization enthalpies etc[]. For example, Landau et al.[] demonstrated that even after the removal of 70% of the virtual space, the errors in the ionization energies of organic compounds were less than 1 kcal/mol. However, it has been well established from previous studies that response properties are usually much more sensitive to the truncation of the wavefunction than simple energetics[]. So we investigated the applicability of such approaches for properties like dynamic polarizabilities using CC linear reponse theory []. In contrast to the earlier studies, we got huge errors in polarizabilities which increased almost

linearly with the number of truncated virtual orbitals. It was found that the ground-state MP2 density used to generate the NOs was unable to capture the response of the wavefunction to the external field. For example, the FVNO procedure threw out first, the diffuse virtual orbitals which are very important to describe the low lying Rydberg type excited states (a common feature in majority of chiral compounds) resulting in large errors. This was not unsurprising since these diffuse orbitals have very low contributions to the correlation energy and hence possess very low occupation numbers. Consistent with the findings of Sundholm and co-workers[**?**], dropping high energy canonical HF virtual orbitals led to very small errors in polarizabilities. We also constructed a first-order perturbed MP2 density hoping that the ONs obtained from this density would be a better metric for estimating the importance of a virtual orbital for response properties but this approach only offered minor improvements over the regular FVNO method. However, a suite of methods, conceptually not very different from our perturbed density approach have been proposed recently to calculate CC excitation energies. Baudin and co-workers used natural transition orbitals (NTOs) obtained from approximate CIS(D) transition densities, a scheme which they call CorNFLEx for calculating CC2 excitation energies of large solvated formamide clusters[]. In similar works, Höfener and Klopper obtained effective virtual spaces by combining MP2 ground state density with excited state densities constructed from CIS excitation vectors[] while Mester et al. used MP2 and CIS(D) amplitudes to define their optimal virtual and occupied spaces[**?**, **?**]. These successful works prompted us to take back a closer look at the reasons behind the failure of our perturbed density approach. Finally, we have developed a

new method which we call FVNO++ where we construct a second-order perturbed density to capture the response of the wavefunction to the external electric and magnetic fields. In this paper, we take a closer look at this scheme and report its performance in calculating CC dynamic polarizabilities and specific rotations of a number of chiral molecules. We also look at the potential applications of this approach to large solvated clusters.

4.2 Theoretical Background

4.2.1 Coupled Cluster Response Theory

The response functions for calculating dynamic higher-order properties can be defined by the frequency dependent coefficients appearing in the expansion of the expectation value of an appropriate time-independent operator in orders of the perturbation.[**?**]

$$\begin{aligned}\langle A\rangle(t) = \langle A\rangle + \int_{-\infty}^{\infty} d\omega_1 \langle\langle A; V^{\omega_1}\rangle\rangle_{\omega_1\ +i\alpha} e^{-i(\omega_1+i\alpha)t} \\ + \frac{1}{2}\int_{-\infty}^{\infty} d\omega_1 \int_{-\infty}^{\infty} d\omega_2\ \langle\langle A; V^{\omega_1}; V^{\omega_2}\rangle\rangle_{\omega_1\ +i\alpha,\omega_2+i\alpha} e^{-i(\omega_1+\omega_2+2i\alpha)t} + ...\end{aligned} \tag{4.1}$$

Here $\langle A\rangle$ is the time independent expectation value and $\langle\langle A; V^{\omega_1}\rangle\rangle_{\omega_1+i\alpha}$ is the linear response function (LRF) i.e. the first order change in the expectation value of A in a time-dependent field V at frequency ω_1. The third term in the expansion contains the quadratic response function and so on. For a CC wavefunction, time-dependent expectation value of A is defined as[**?**],

$$\begin{aligned}\langle A\rangle_{CC}(t) =& Re[\langle\Lambda(t)|A|CC(t)\rangle] \\ &= \frac{1}{2}(\langle\Lambda(t)|A|CC(t)\rangle + \langle\Lambda(t)|A|CC(t)\rangle^*)\end{aligned} \tag{4.2}$$

where $\langle\Lambda(t)|$ and $|CC(t)\rangle$ are the left and right time dependent phase-isolated CC wavefunction, parametrized as,

$$\begin{aligned}\langle\Lambda(t)| &= \langle 0| + \sum_{\mu}\lambda_{\mu}(t)\langle\mu|e^{-T(t)} \\ |CC(t)\rangle &= e^{T(t)}|0\rangle.\end{aligned} \tag{4.3}$$

where μ refers to excited determinants i.e. singles, doubles etc., and $|0\rangle$ is the reference wavefunction. To identify CC response functions one needs to expand $\langle\Lambda(t)|A|CC(t)\rangle$ in orders of perturbation[**?**],

$$\begin{aligned}\langle\Lambda(t)|A|CC(t)\rangle &= \langle\Lambda(t)|A|CC(t)\rangle^{(0)} + \langle\Lambda(t)|A|CC(t)\rangle^{(1)} + \langle\Lambda(t)|A|CC(t)\rangle^{(2)} + ... \\ &= \langle\Lambda|A|CC\rangle + \int_{-\infty}^{\infty} d\omega_1\ F^{A;V^{\omega_1}}_{\omega_1+i\alpha}e^{-i(\omega_1+i\alpha)t} \\ &+ \frac{1}{2}\int_{-\infty}^{\infty}d\omega_1\int_{-\infty}^{\infty}d\omega_2\ F^{A;V^{\omega_1};V^{\omega_2}}_{\omega_1+i\alpha,\omega_2+i\alpha}e^{-i(\omega_1+\omega_2+2i\alpha)t} + ...\end{aligned} \tag{4.4}$$

From eqns 4.1-4.4 and using the relation $F^{B;A}_{-\omega_1} = F^{A;B}_{\omega_1}$, the CC-LRF can be identified as

$$\langle\langle A; V^{\omega_1}\rangle\rangle_{\omega_1+i\alpha} = \frac{1}{2}(F^{A;V^{\omega_1}}_{\omega_1+i\alpha} + (F^{V^{\omega_1};A}_{\omega_1+i\alpha})^*) \tag{4.5}$$

Alternatively, LRFs can also be defined as second-order derivatives of a time-averaged quasi-

energy with respect to external perturbations $\hat{A}$ and $\hat{B}$. This formalism is specially useful for deriving LRFs for approximate coupled cluster theories like CC2, CC3 etc. The electric-electric (α) and electric-magnetic (β) dipole polarizability tensor elements can be obtained from the LRF with appropriate operators,

$$\alpha_{xy}(\omega) = \langle\langle \mu_x; \mu_y \rangle\rangle_{\omega_1} \tag{4.6}$$

$$\beta_{xy}(\omega) = -\mathrm{Im}\langle\langle \mu_x; m_y \rangle\rangle_{\omega_1} \tag{4.7}$$

where $\boldsymbol{\mu} = \sum_i q_i \boldsymbol{r_i}$ and $\boldsymbol{m} = \sum_i \frac{q_i}{2m_i} \boldsymbol{r_i} \times \boldsymbol{p_i}$. Isotropic electric dipole polarizability is one-third of the trace of the α tensor while specific rotation is related to the one-third of the trace of the β tensor (au) also known as the Rosenfeld tensor normalized by the path-length and concentration[],

$$[\alpha]_\omega = \frac{(72.0 \times 10^6)\hbar^2 N_A \omega}{c^2 {m_e}^2 M} \times \left[\frac{1}{3} Tr(\beta)\right] \tag{4.8}$$

where M is the mass of the molecule (amu), m_e is the rest mass of an electron (kg), c is the speed if light in vacuum (m/s), N_A is Avogadro's number and ω is the frequency of the electromagnetic field (au).

Following is the final simplified expression of CC-LRF[]:

$$\langle\langle A; B \rangle\rangle_{\omega_1} = \frac{1}{2}\hat{P}(A,B)[\langle 0| \ [\hat{Y}^B_{\omega_1}, \bar{A}]|0\rangle + \langle 0| \ (1+\hat{\Lambda})|[\bar{A}, \hat{X}^B_{\omega_1}]|0\rangle] \tag{4.9}$$

where A and B are the one electron perturbation operators, $\hat{P}(A,B)$ simultaneously interchanges operators A and B and takes the complex conjugate of the expression, ω_1 is the frequency of the external field, $|0\rangle$ is the reference wavefunction, $\hat{\Lambda}$ is a linear de-excitation operator that parametrizes the CC left hand wavefunction to make sure that the CC gradients satisfy the generalized Hellman-Feynman theorem[], overbar on operataor A denotes similarity transformation with the ground state T operator, $\bar{A} = e^{-\hat{T}}\hat{A}e^{\hat{T}}$ and $\hat{X}^B_{\omega_1}$ and $\hat{Y}^B_{\omega_1}$ are excitation operators involving the first-order right and left hand perturbed amplitudes corresponding to operator B respectively. These amplitudes can be obtained by solving a linear system of equations,

$$\begin{aligned}
&\sum_{\nu}\langle\mu|\big[(\bar{H}-\omega I),\tau_\nu\big]|0\ \rangle X^B_\nu = -\langle\mu|\bar{B}|0\rangle \\
&\sum_{\nu} Y^B_\nu\langle\nu|\big[(\bar{H}+\omega I),\tau_\mu\big]|0\rangle\ + \langle 0|(1+\hat{\Lambda})|\big[\big[\bar{H},\tau_\nu\big],\tau_\mu\big]|0\rangle\ X^B_\nu = -\langle 0|(1+\hat{\Lambda})|\big[\bar{B},\tau_\mu\big]|0\rangle
\end{aligned} \tag{4.10}$$

Here τ_μ, τ_ν are excitation operators which when act on the reference wavefunction $|0\rangle$ create excited determinats $|\mu\rangle$ and $|\nu\rangle$ respectively. Also, the dependence of perturbed amplitudes on ω_1 is assumed. The right hand amplitudes are solved first after which they enter into the left hand amplitude equations as inhomogenous terms. It should be noted that these equations need to be solved for every cartesian component of the given perturbation operators. For example, calculation of optical rotation tensor using length-gauge representation of the

dipole operator would require solving a total of 12 linear equations, six each for both electric and magnetic dipole perturbation.

4.2.2 Perturbed Natural Orbitals

The CC-LRF (eq. 4.9) can also be formulated in terms of perturbed densities,

$$\langle\langle A; B\rangle\rangle_{\omega_1} = \frac{1}{2}\hat{P}(A,B)\big[\sum_{pq} A_{pq}[D_{pq}^{B^{\omega_1}}]^{(1)}\big] \tag{4.11}$$

where $[D^{B^{\omega_1}}]^{(1)}$ is the frequency dependent first-order perturbed one-electron density related to operator B. The structures of the virtual-virtual block of perturbed densities of different orders (for a given perturbation operator) can be easily identified in spin orbitals,

$$\begin{aligned}
D_{ab}^{(0)} &= \frac{1}{2}(\lambda_{ac}^{ij})^{(0)}(t_{ij}^{bc})^{(0)} \; + (\lambda_a^i)^{(0)}(t_i^b)^{(0)} \\
D_{ab}^{(1)} &= \frac{1}{2}[(\lambda_{ac}^{ij})^{(0)}(t_{ij}^{bc})^{(1)} \; + (\lambda_{ac}^{ij})^{(1)}(t_{ij}^{bc})^{(0)}] + [(\lambda_a^i)^{(0)}(t_i^b)^{(1)} \; + (\lambda_a^i)^{(1)}(t_i^b)^{(0)}] \\
D_{ab}^{(2)} &= \frac{1}{2}[(\lambda_{ac}^{ij})^{(1)}(t_{ij}^{bc})^{(1)} \; + (\lambda_{ac}^{ij})^{(0)}(t_{ij}^{bc})^{(2)}] \; + [(\lambda_a^i)^{(1)}(t_i^b)^{(1)} + (\lambda_a^i)^{(0)}(t_i^b)^{(2)}].
\end{aligned} \tag{4.12}$$

In the above equation, the indices i, j and a, b, c refer to occupied and virtual orbitals respectively and Einstein summation notation is used. The first order perturbed amplitudes $(\lambda_{ac}^{ij})^{(1)}$ and $(t_{ij}^{bc})^{(1)}$ are nothing but the $\hat{X}_{\omega_1}^B$ and $\hat{Y}_{\omega_1}^B$ amplitudes that we saw earlier.

Just as the ground state MP2 density can transfer its knowledge of electron correlation effects to the one electron basis (virtual NOs) through diagonalization, the perturbed densities can be used in a similar way to construct a compact "perturbation aware" basis. In our earlier work, we constructed a guess first-order pertubed density associated with each

cartesian component (x,y,z) of the perturbation operator (dipole in the case of polarizabilities) from MP2 amplitudes, took an average of the three densities and then diagonalized it to obtain our virtual space but this approach offered only a minor improvement[]. To investigate the reason behind the failure of this model, we constructed the virtual-virtual block of the full CCSD first-order perturbed density. All the diagonal elements of this density matrix were found to be zeros irrespective of the perturbation operator. The exact reason for this is not yet understood but clearly, the virtual NOs (VNOs) obtained from this (or guess) density doesn't carry any useful information. However, since the polarizabilities and specific rotations are second-order in perturbation, second-order perturbed densities should in principle be a better metric for estimating the importance of a VNO for these properties. In this paper, we use an average of second-order guess densities corresponding to each cartesian component of an appropriate perturbation operator to define our virtual space for correlated response calculations. For a perturbation operator A, this guess density looks like,

$$[D^A_{ab}]^{(2)} = \frac{1}{2}[t^{ac}_{ij}(A)]^{(1)}[t^{bc}_{ij}(A)]^{(1)} \ + [t^a_i(A)]^{(1)}[t^b_i(A)]^{(1)}, \tag{4.13}$$

where,

$$\begin{aligned} t^{ac}_{ij}(A)^{(1)} &= \frac{\bar{A}^{ac}_{ij}}{\epsilon_a + \epsilon_c - \epsilon_i - \epsilon_j}, \\ t^a_i(A)^{(1)} &= \frac{\bar{A}^a_i}{\epsilon_a - \epsilon_i} \end{aligned} \tag{4.14}$$

Here, we have used MP2 amplitudes for the similarity transformation,

$$\bar{A}^{ac}_{ij} = P^{ac}_{ij}(t^{ec}_{ij}A^a_e - t^{ac}_{mj}A^m_i), \tag{4.15}$$

ignored the terms involving second-order perturbed amplitudes and approximated the first-order perturbed λ amplitudes with the corresponding t amplitudes. The equations for solving the first-order right-hand perturbed amplitudes (eq. 4.10) can also be written in terms of the inverse of the CC Jacobian,

$$\begin{aligned} t_{ij}^{ac}(A)^{(1)}(\omega_1) &= \sum_{\mu} -\langle \Phi_{ij}^{ac}|(\bar{H} - \omega_1 I)^{-1}|\mu\rangle\langle\mu|\bar{A}|0\rangle, \\ t_{i}^{a}(A)^{(1)}(\omega_1) &= \sum_{\mu} -\langle \Phi_{i}^{a}|(\bar{H} - \omega_1 I)^{-1}|\mu\rangle\langle\mu|\bar{A}|0\rangle \end{aligned} \tag{4.16}$$

It can be clearly seen that the guesses for $t_{ij}^{ac}(A)^{(1)}$ and $t_{i}^{a}(A)^{(1)}$ amplitudes in this work have been chosen by only considering the diagonal elements of $(\bar{H} - \omega_1 I)^{-1}$ which can be justified due to the diagonally dominant nature of the $\bar{H}$ matrix. Furthermore, we keep ω_1 as zero as we want to use the same density matrix for a given property calculation at different frequencies. We also assume that removing ω_1 should not significantly change the sparsity pattern of the perturbed amplitudes. Finally, the basic outline of this approach involves doing a MP2 calculation, generation of guess densities using MP2 amplitudes and perturbation operators, diagonalization of the virtual-virtual block of the guess density to obtain VNOs, truncation of VNOs with occupation numbers below a given threshold, diagonalization of the Fock matrix in the truncated VNO basis to obtain a semi-canonical basis, transformation of all the one and two electron integrals to this semi-canonical basis, followed by CC2/CCSD-LR calculations at given frequencies.

4.3 Computational Details

The main target of this work is large scale CC2/CCSD calculations of specific rotations of solvated molecular clusters. However, first, we need to ensure that the FVNO++ approach has the right convergence behavior towards the full canonical result. In this regard, we carry out dynamic polarizabilities and specific rotation calculations of a number of small and medium sized chiral molecules ranging from linear hydrogen dimer (P)-$(H_2)_n$ helices and (M)-1-Fluoralkanes to (S)-1-Phenylethanol, a molecule having two-dimensional structure and ultimately molecules with cagelike structutes: (1R,4R)-Norbornenone and (1R,5R)-β-Pinene.

4.3.1 Polarizabilities

Polarizability calculations on these chiral molecules can be as seen as a diagnostic tool for gaining insight into the nature of specific rotation calculations as one truncates the virtual space as even though the response functions of both the properties are quite similar, polarizabilities are much less sensitive to the wavefunction truncation. In all the polarizability calculations, the length-gauge (LG) representation of the electric dipole operator was used. The natural choice of perturbed densities for such calculations is : $\sum_q \frac{1}{3}[D_{ab}^{\mu_q}]^{(2)}$, where $q \equiv [x, y, z]$.

4.3.2 Specific Rotations

For specific rotation calculations, we employed both the LG and modified velocity gauge (MVG)[] representations. If we consider the LG calculations, there is no obvious choice of how to construct perturbed densities. Both $[D_{ab}^{\mu_q}]^{(2)}$ and $[D_{ab}^{m_q}]^{(2)}$ are valid choices. Hence, we use both the densities for defining our virtual space and compare their performances. Similarly, in MVG calculations, we use both $[D_{ab}^{p_q}]^{(2)}$ and $[D_{ab}^{m_q}]^{(2)}$ as our definitions of perturbed densities where p is the momentum operator, i.e. $p_q = -i\frac{\partial}{\partial q}$. The primary basis set used in this work is aug-cc-pVDZ[] and all the property calculations were carried out at 589 nm using using Psi4 and Psi4Numpy software packages.[] We also report the sparsity pattern of the guess densities of large solvated molecular clusters using DF-MP2 which give us an estimate of the computational savings that can be exploited for such systems. It should be noted that we have used the same virtual space for calculating both unperturbed and perturbed amplitudes as this ensures a match with results obtained from the finite-field procedures.

4.4 Results and Discussion

Retention of diffuse space: Sort all the canonical MOs by their spatial extents ¡i—r*r—i¿, choose a cutoff, retain all the orbitals above that cutoff and apply the regular FVNO in the remaining virtual space. As an example for h2o2 in aug-cc-pvdz basis., we retained 26 out of 55 most diffuse virtual CMOs, constructed MP2 ground state density in the remaining space of 29 virtual orbitals. Fig.1 compares the performance of this method with the regular FVNO

approach for calculating CCSD dynamic polarizabilities and specific rotation at 589 nm. Explain the trend - minimal errors. Similar errors can be expected for a lot of chiral molecules who like h2o2 possess low lying Rydberg states. However, such a simplified approach could mean retaining a lot of diffuse virtual orbitals which might not be feasible for large-scale calculations. Moreover, the metric of retention might be not well-defined. Thus, we instead look at the performance of the second-order perturbed density approach which we have named as FVNO++ in the next sections.

4.4.1 $(H_2)_n$ Helices

- Linear structure, chiral, helical arrangement - best case for local correlation problems - small masses, high OR - Polariz, specific rotation (h2)4, (h2)5, (h2)6, (h2)7, maybe-bigger!! : LG, MVG, aDZ basis - diagnostics for FVNO++ approach: - first comparing the structure of the ground state and perturbed density, one can see that perturbed density would have a higher rank than ground-state density. - how about incorporating L*L density as well and optimized NOs by better guess densities. - Here we mostly concentrate on capturing the right kind of behavior rather than savings, since there is not enough sparsity on offer for these cases. This is applicable for other test cases as well.

4.4.2 beta-pinene

4.4.3 phenyl-ethanol

4.4.4 norbornenone

Maybe bring MP2 diagnostics here as a reason for poor behavior! I mean here the pi-pi* excitations might require accurate T2 amplitudes as well.

4.4.5 Sparsity in solvated cluster

4.5 Conclusions

- Within the FVNO++ formalism, explored structures of second-order perturbed densities: Dab(2)(MU), Dab(2)(P), Dab(2)(MU,L), Dab2(P,L), Dab(2)(L) employing different guesses of first-order perturbed amplitudes. Based on plot studies on small systems, we can conclude that this approach works, has the right behavior/convergence properties. however, as usual, specific rotation is more sensitive than polarizabilities and requires bigger virtual spaces. Real application is solvated clusters, where we conclude that there is a lot of sparsity to take advantage of. Thus, we are going to implement RI-CC2 linear response in conjunction with the FVNO++ aproach. Also, this could easily be extended to PNO aproaches for reduced scaling.

4.6 Acknowledgements

Chapter 5

Perturbed Pair Natural Orbitals for Coupled-Cluster Linear-Response Theory

5.1 Introduction

Accurate *ab initio* models like the coupled cluster theory have been used quite reliably to predict the chiroptical properties of molecules.[] However, they have been limited to very small system sizes due to the heavy computational expenses associated with such methods. For example, the coupled cluster singles and doubles method (CCSD) has a high polynomial scaling of $O(N^6)$, where N is some measure of the system size. This is clearly unphysical

as the phenomenon of dynamic electron-correlation, which these methods aim to capture, is local in nature.[] This steep scaling can be attributed to the use of delocalized canonical Hartree-Fock MOs (CMOs) as the one electron basis for representing the wavefunction. Local correlation techniques try to exploit the intrinsic sparsity in correlated wavefunctions by unitarily localizing the occupied orbitals (LMOs) using methods like Boys-Foster, Pipek-Mezey etc[]. and constructing excitation domains corresponding to each LMO. The sizes of these domains are usually very small compared to the full virtual space and become constant in the asymptotic limit, making these approaches reduced-scaling. Saebo and Pulay's introduction of projected atomic orbitals (PAO) as a representation of the virtual space stands as one of the earliest works in this regard[]. As the name suggests, PAOs are formed by projecting out the occupied MO components from the AO basis. Since the PAOs are centered on atoms (just like AOs), an excitation domain for a given LMO can be constructed by including only those PAOs which are on or near the atoms associated with that LMO. Subsequently, domains corresponding to a pair of LMOs can be formed by taking a union of the PAO space of both the LMOs and so on. Werner, Schütz and co-workers [] were the first to apply these concepts within the framework of CC theory. By employing truncated PAO domains coupled with other approximations like weak and distant pairs, they were able to achieve linear scaling while maintaining accurate description of ground-state properties like reaction enthalpies, thermodynamic constants etc.[] Crawford and King were the first to use PAOs with the equation of motion CCSD method to calculate excitation energies[]. In a similar work, Korona and Werner[] by constructing state specific PAO domains minimized

the average localization errors for their test set to only 0.06 ev. Schutz and co-workers extended this approach with density-fitted second order coupled cluster (CC2) [] method to calculate excited state properties of large systems.[] However, these approaches could require very large domian sizes depending on the character of the excited state, for example, excitations in a charge-transfer excited state could be fairly non-local. PAOs have also been used within the context of CC linear response theory to calculate higher-order response properties like (hyper)polarizabilities, chiroptical response etc. albeit on a much smaller scale.[] In 2004, Korona and Werner[] used PAOs with local coupled cluster singles and doubles method (LCCSD) to calculate electric dipole moments and static polarizabilities where they got average errors of 1.61% and 0.48% respectively. Further minimization of the errors required building bigger domains leading to a significant increase in computational expenses. In the same year, Russ and Crawford[] used a modified domain building procedure within the PAO framework, where they augmented the ground state orbital domains on the basis of first-order orbital response coefficients obtained by sloving the coupled-perturbed Hartree-Fock equations, to calculate CC static polarizabilities. A few years later, they extended this formalism to calculate dynamic polarizabilities and optical rotations[]. While the localization errors for linear molecular structures were shown to be only a few percent of canonical results, three dimensional compounds required very large domains, specially for optical rotations. A similar conclusion was drawn when Friedrich and co-workers applied the incremental scheme, a fragmentation based local correlation technique to calculate CC dynamic polarizabilities.[] For a more detailed overview of the applications of PAO based methods in this field, please

refer to ref[**?**]. Within the framework of local correlation, the pair natural orbitals (PNOs) introduced in 1970s by Edimnston and Krauss[], Meyer[], Ahlrichs[], Kutzelnigg[], Staemmler and co-workers[] and orbital specific virtuals (OSVs) developed by Chan and co-workers in 2011 [], are other popular alternatives to PAOs for a compact representation of the virtual space. In the local PNO (LPNO) approach, each pair of LMOs have their own virtual space which can be obtained by the diagonalization of the virtual-virtual block of an approximate 1-electron pair specific density. The OSV approach on the other hand involves diagonalization of a separate density for each LMO. Even though the PNOs were shown be to be quite useful as a wavefunction compression technique[], they were initially abandoned due to the computational costs involved in the transformation of the two electron integrals, onlyto be revived later by Neese and co-workers in 2008 by making use of the density-fitting procedure []. They also proposed a variant of the LPNO approach, a scheme which they call domain based LPNO (DLPNO), where the PNOs are expressed in terms of PAOs, to achieve near-linear scaling behavior in MP2 and CC calculations []. Following their pioneering works, the LPNO and the DLPNO methods has been used quite sucessfully to study ground state properties of molecular systems previously unreachable by canonical correlated methods[]. [] Hattig and co-workers were the first to extend this scheme to excited states by using state-specific PNOs generated from CIS(D) densities at CC2 level of theory[] and recently with CCSD.[]. Valeev and co-workers recently implemented a state-averaged L-PNO-CCSD simulation program by taking an average of the CIS(D) densities over a desired set of excited states[]. Similar works employing state-specific natural transition orbitals and natural orbitals for calculating

excitation energies have also been reported. [] Our group implemented the LPNO scheme in conjunction with CC2 and CCSD linear response (LR) theory to calculate dynamic polarizabilities and specific rotations of different chiral molecules ranging from linear (H2)n helices to cagelike 1r-4r-norbornenone, where consistent with earlier studies, PNOs were found to be much more compact than the PAOs and OSVs for representing the wavefunction. However, the truncation errors in specific rotations for 3-dimensional structures were quite large and the convergence of both the properties towards the canonical result turned out to be very slow[]. The failure of the regular LPNO-CC2/CCSD-LR approach for higher-order response properties could be attributed to the inability of the ground-state MP2 density to capture the response of the wavefunction, as shown in our earlier work with natural orbitals (NOs)[]. However, we have recently demonstrated that the NOs obtained from "perturbation aware" densities are better suited for calculating these response properties.[] In this paper, we extend this approach which we have named PNO++ by constructing second-order pair specific perturbed densities, and compare its performance with the regular method for the same test systems as our earlier PNO paper.

5.2 Theory

5.2.1 Coupled Cluster Response Theory

Coupled cluster (CC) response theory has been proven to be quite a reliable and accurate theoretical tool to calculate higher-order response properties[]. Within this formalism, one expands the time-dependent expectation value of a time-independent operator in different orders of the perturbation. The response functions can then be identified as fourier analogues (FA) of the time-dependent expansion terms up to a given order, ex. the linear response function (LRF) is the FA of terms appearing in the first order in the expansion. CC-LRF for time independent operators A and B can be written as[],

$$\langle\langle A;B\rangle\rangle_{\omega_1} = \frac{1}{2}\hat{P}(A,B)[\langle 0|\ [\hat{Y}^B_{\omega_1},\bar{A}]|0\rangle + \langle 0|\ (1+\hat{\Lambda})|[\bar{A},\hat{X}^B_{\omega_1}]|0\rangle] \tag{5.1}$$

where $\hat{P}(A,B)$ is a symmetrizing operator which simultaneously interchanges operators A and B and takes the complex conjugate of the expression, ω_1 is the frequency of the external field, $|0\rangle$ is the reference wavefunction, $\hat{\Lambda}$ is a linear de-excitation operator that parametrizes the CC left hand wavefunction, overbar on operator A denotes a similarity transformation with the ground state T operator, $\bar{A} = e^{-\hat{T}}\hat{A}e^{\hat{T}}$ and $\hat{X}^B_{\omega_1}$ and $\hat{Y}^B_{\omega_1}$ are the first-order right and left hand perturbed amplitudes corresponding to perturbation operator B respectively. The LRF expression above can be re-written in terms of frequency-dependent first-order perturbed densities $D^{B^{\omega_1}(1)}_{pq}$,

$$\begin{aligned}\langle\langle A;B\rangle\rangle_{\omega_1} &= \frac{1}{2}\hat{P}(A,B)[\sum_{pq} A_{pq}\langle 0|\ \hat{Y}^B_{\omega_1}, \overline{a^\dagger_p a_q}]|0\rangle + \langle 0|\ (1+\hat{\Lambda})|[\overline{a^\dagger_p a_q}, \hat{X}^B_{\omega_1}]|0\rangle] \\ &= \frac{1}{2}\hat{P}(A,B)\big[\sum_{pq} A_{pq}[D^{B^{\omega_1}}_{pq}]^{(1)}\big]\end{aligned} \tag{5.2}$$

where $a^\dagger_p$ and a_q are creation and annihilation operators respectively. In spin orbitals, the virtual-virtual block of this density looks like,

$$D^{B^{\omega_1}(1)}_{ab} = \frac{1}{2}\sum_{ijc}[\lambda^{ij}_{ac}X^{bc}_{ij}\ + Y^{ij}_{ac}t^{bc}_{ij}] + \sum_{i}[\lambda^{i}_{a}X^{b}_{i}\ + Y^{i}_{a}t^{b}_{i}] \tag{5.3}$$

where X and Y are the right and left hand first order perturbed amplitudes associated with perturbation B at frequency ω_1. These amplitudes can be obtained by solving a linear system of equations,

$$\begin{aligned}\sum_{\nu}(\bar{H}-\omega I)_{\mu\nu}X^B_\nu &= -\bar{B}_\mu \\ \sum_{\nu}Y^B_\nu(\bar{H}+\omega I)_{\nu\mu} &= -\sum_{\nu}X^B_\nu F'_{\nu\mu} - \bar{B}'_\mu\end{aligned} \tag{5.4}$$

where,

$$\begin{aligned}(\bar{H}\pm\omega I)_{\mu\nu} &= \langle\mu|\big[(\bar{H}\pm\omega I),\tau_\nu\big]|0\rangle \\ F'_{\nu\mu} &= \langle 0|(1+\hat{\Lambda})|\big[\big[\bar{H},\tau_\nu\big],\tau_\mu\big]|0\rangle \\ \bar{B}_\mu &= \langle\mu|\bar{B}|0\rangle \\ \bar{B}'_\mu &= \langle 0|(1+\hat{\Lambda})|\big[\bar{B},\tau_\mu\big]|0\rangle.\end{aligned} \tag{5.5}$$

Here τ_μ, τ_ν are operators which generate excited determinats $|\mu\rangle$ and $|\nu\rangle$ by acting on the reference wavefunction $|0\rangle$. Once, we solve for X_ν^B and Y_ν^B amplitudes, the first-order perturbed density can be built from eq.(5.3) to construct the CC-LRF. Elements of the dynamic polarizability ($\boldsymbol{\alpha}$) and optical rotation ($\boldsymbol{\beta}$) tensors can be obtained from the LRF with appropriate perturbation operators. For example,

$$\begin{aligned} \alpha_{xy}(\omega) &= \langle\langle \mu_x; \mu_y \rangle\rangle_{\omega_1} \\ \beta_{xy}(\omega) &= -\mathrm{Im}\langle\langle \mu_x; m_y \rangle\rangle_{\omega_1} \end{aligned} \tag{5.6}$$

where $\boldsymbol{\mu} = \sum_i q_i \boldsymbol{r_i}$, $\boldsymbol{m} = \sum_i \frac{q_i}{2m_i} \boldsymbol{r_i} \times \boldsymbol{p_i}$ and "Im" signifies that $\beta_{xy}(\omega)$ equals the imaginary part of the corresponding LRF.

5.2.2 Ground State PNOs

The first step in any local correlation approach is the induction of sparsity in the occupied space. Standard techniques like Boys-Foster, Pipek-Mezey accomplish this by producing localized MOs or LMOs. The PNOs for a given pair of LMOs ij can then be defined by a unitary rotation of the virtual orbitals,

$$|\bar{\boldsymbol{a}}^{ij}\rangle = \sum_a |a\rangle \boldsymbol{Q}_{a\bar{a}}^{ij} \tag{5.7}$$

where the transformation matrix $\boldsymbol{Q}_{a\bar{a}}^{ij}$ is the eigenvector of the pair ij's contribution to the virtual-virtual block of the one electron density matrix (1-RDM) i.e $\boldsymbol{D} = \sum_{ij} [\boldsymbol{D}^{ij}]$.

$$\boldsymbol{D}^{ij} \boldsymbol{Q}^{ij} = \boldsymbol{Q}^{ij} \boldsymbol{n}^{ij} \tag{5.8}$$

The eigenvalues $\boldsymbol{n}^{ij}$ are referred to as "occupation numbers" (ONs) and can be seen as a metric for estimating the importance of the corresponding PNO for describing electron correlation effects for the pair ij. For CCSD/CC2 ground state calculations, approximate pair densities are usually formed from the MP2 amplitudes,

$$\boldsymbol{D}^{ij} = \frac{2}{1+\delta_{ij}}(\boldsymbol{T}^{ij}\tilde{\boldsymbol{T}}^{ij\dagger} + \boldsymbol{T}^{ij\dagger}\tilde{\boldsymbol{T}}^{ij}) \tag{5.9}$$

where,

$$\begin{aligned} \tilde{\boldsymbol{T}}^{ij} &= 2\boldsymbol{T}^{ij} - \boldsymbol{T}^{ij\dagger} \\ T^{ij}_{ab} &= \frac{\langle ab|ij\rangle}{f_{ii} + f_{jj} - \epsilon_a - \epsilon_b}. \end{aligned} \tag{5.10}$$

Here, indices i, j, k and a, b, c have been used for occupied and virtual orbitals respectively. The integrals $\langle ab|ij\rangle$ are in physicist notation, f_{ii} and f_{jj} are the i^{th} and j^{th} diagonal elements of the Fock matrix in the LMO basis and ϵ_a, ϵ_b are the orbital energies of the canonical virtual orbitals a and b respectively. The PNOs with ONs smaller than a given threshold (usually in $10^{-6} - 10^{-8}$ range) are then neglected as they have minimal contributions to the total correlation energy. Finally, the canonical CC2/CCSD equations are reformulated or refactored in terms of these truncated PNO transformations. It should be noted that the virtual spaces of different pairs of LMOs are non-orthogonal to each other due to which the transformation of amplitudes from one pair to another requires a overlap metric given by,

$$\boldsymbol{S}^{ij,kl} = \boldsymbol{Q}^{ij\dagger}\boldsymbol{Q}^{kl} \tag{5.11}$$

5.2.3 Perturbed PNOs

It was shown from our earlier work that the regular LPNO-[CCSD/CC2]-LR approach has very slow convergence towards the full canonical result both for dynamic polarizabilities and specific rotations[]. This is unsurprising since the sparsity of perturbed and unperturbed amplitudes are usually very different from each other. Thus, the pair densities should be able to capture the response of the ground state amplitudes. Recent reduced scaling works on ADC(2) or EOM-CC2/CCSD excitation energies employ PNO-MP2 and PNO-CIS(D) densities for ground and excited state calculations respectively.[] However, for caluclating response properties using CC-LR theory, one needs to express both unperturbed and perturbed amplitudes in the same PNO basis in order to match the results obtained from finite field procedures. Due to this constraint, two different schemes could be explored where a) PNOs are defined from perturbed densities b) effective PNOs are obtained by a union of truncated PNOs defined from MP2 and perturbed densities. It should be noted that one can't just add ground state and perturbed densities together to define an effective density as they are not in the same units. We have implemented scheme a) in this work and call it LPNO++. This approach can be justified due to the fact that our target is not total energies but the derivative of the total energies in the presence of external fields. Furthermore, it can be shown that on replacing the CC ground state amplitudes with that of MP2 in CC-LR theory one introduces minimal errors for both polarizabilities and specific rotations.[] Hence, even though LPNO++ can't be expected to work as well as LPNO for ground state calculations, it can capture the response of the wavefunction very efficiently and hence

should perform a lot better for these kinds of properties. The LPNO++ approach involves creation of a perturbation specific density for each ij pair. This is an extension of our work on natural orbitals where we showed that second-order perturbed densities can be used quite efficiently for calculating response properties[]. For a given perturbation A, the LPNO++ density is constructed by replacing the MP2 T_{ab}^{ij} amplitudes by the corresponding perturbed amplitudes X_{ab}^{ij}.

$$\boldsymbol{D}^{A;ij} = \frac{2}{1+\delta_{ij}}(\boldsymbol{X}^{ij}\tilde{\boldsymbol{X}}^{ij\dagger} + \boldsymbol{X}^{ij\dagger}\tilde{\boldsymbol{X}}^{ij}) \tag{5.12}$$

Rewriting the first part of eq.(5.4),

$$X_{\mu}^{A} = -\sum_{\nu} \left(\bar{H} - \omega I\right)^{-1}{}_{\mu\nu}\bar{A}_{\nu} \tag{5.13}$$

one can see that an obvious guess for X_{ab}^{ij} amplitudes could be constructed as

$$X_{ab}^{ij} = \frac{\bar{A}_{ab}^{ij}}{f_{ii} + f_{jj} - \epsilon_a - \epsilon_b} \tag{5.14}$$

since the leading contribution to the inverse of the diagonally dominant $(\bar{H} - \omega I)$ matrix would come from the inverse of its diagonal elements, i.e. $f_{ii} + f_{jj} - \epsilon_a - \epsilon_b$. Also, $\bar{A}$ has been approximated by using MP2 amplitudes for the similarity transformation,

$$\begin{gathered}\bar{A}_{ab}^{ij} = P_{ij}^{ab}\left[\sum_{e} t_{eb}^{ij}[A_e^a - t_a^m A_e^m] - \sum_{m} t_{ab}^{mj}[A_i^m - t_e^i A_e^m]\right] \\ P_{ij}^{ab} f_{ij}^{ab} = f_{ij}^{ab} + f_{ji}^{ba}\end{gathered} \tag{5.15}$$

Furthermore, we have taken $omega_1$ as zero so that we can use the same density for response calculations at multiple frequencies. This can be justified as the sparsity of the perturbed

amplitudes should more or less stay the same at the frequencies we are interested in. In this approach, the weak pair approximation can also be employed by using a pair-pseudoresponse metric,

$$e_{ab}^{A} = \sum_{ij} \bar{A}_{ab}^{ij} \tilde{\boldsymbol{X}}_{ab}^{ij}. \tag{5.16}$$

All the pairs whose pseudoresponses are below a given threshold can be considered as weak pairs and neglected.

5.3 Computational Details

The ultimate goal of this work is to be able to carry out response calculations of large solvated molecular clusters. for which one would need a production level CC2/CCSD-LPNO++-LR code. As can be seen from eq (5.4), such a code would involve reconstruction of $\bar{H}$ elements in every iteration of response equations from the density-fitted 3-centered integrals. However, before investing a lot of time and effort in this regard, we use a simulation code in this work to test if the LPNO++ approach can offer a more compact virtual space for calculating these properties. As a result, we mostly focus on small chiral systems of varying topologies: (linear) (P)-$(H_2)_n$ helices and (M)-1-Fluoralkanes, (two-dimensional) (S)-1-Phenylethanol, (three-dimensional cagelike) (1R,4R)-Norbornenone and (1R,5R)-β-Pinene. Dynamic polarizabilities and specific rotations calculations are carried out for all of these systems within the CC2,CCSD-LR formalism with aug-cc-pVDZ[] basis set at 589 nm using Psi4 and Psi4Numpy software packages[]. Furthermore, the electric dipole operator μ

is represented in length gauge (LG) for polarizabilities while for specific rotations both LG and modified velocity gauge (MVG)[] representations are used. The choice of perturbed pair density for polarizabilities are pretty straightforward as its LRF only involves the electric dipole operator. Thus, one takes an average of the density corresponding to this operator over all cartesian compoments to define our virtual space. i,e. $\boldsymbol{D}^{\mu;ij} = \sum_q \frac{1}{3}[\boldsymbol{D}^{\mu_q;ij}]$, where $q \equiv [x, y, z]$. Since, specific rotation's LRF has both electric and magnetic dipole operators, we use the associated densities individually and compare their performances in this work. As the MVG representation expresses electric dipole in terms of the momentum operator $\hat{p}$, we use $\boldsymbol{D}^{p;ij}$ instead of $\boldsymbol{D}^{\mu;ij}$.

One of the advantages of the simulation code is that it requires minimal changes in the canonical CCLR code. In this procedure, the residual of the CC amplitude equations, (R^{ij}, R^i) is transformed from the canonical MO basis to the PNO basis in every iteration.

$$\begin{aligned} \boldsymbol{R}^{ij} &= \boldsymbol{Q}^{ij\dagger} R^{ij} \boldsymbol{Q}^{ij} \\ \boldsymbol{R}^{ii} &= \boldsymbol{Q}^{ii\dagger} R^{i} \boldsymbol{Q}^{ii} \end{aligned} \tag{5.17}$$

One can can continue to work in the PNO basis but since the virtual-virtual block of the Fock matrix is not diagonal in this basis, the convergence of the amplitude equations is expected to be slower. Thus, its common to use a semicanonical PNO basis which diagonalizes $\boldsymbol{F}^{ij}_{vir}$,

$$\begin{aligned} \boldsymbol{U}^{ij\dagger} \boldsymbol{F}^{ij}_{vir} \boldsymbol{U}^{ij} &= \boldsymbol{\Lambda}^{ij} \\ \bar{\boldsymbol{R}}^{ij} &= \boldsymbol{U}^{ij\dagger} \boldsymbol{R}^{ij} \boldsymbol{U}^{ij} \\ \bar{\boldsymbol{R}}^{ii} &= \boldsymbol{U}^{ii\dagger} \boldsymbol{R}^{ii} \boldsymbol{U}^{ii} \end{aligned} \tag{5.18}$$

where $\mathbf{\Lambda}^{ij}$ is the diagonal matrix containing orbital energies ($\boldsymbol{\epsilon}_a^{ij}$, $\boldsymbol{\epsilon}_b^{ij}$, ..). Subsequently, the preconditioner is applied to the residual to calculate the increment,

$$\begin{aligned} \bar{\mathbf{\Delta}}^{ij} &= \frac{\bar{\boldsymbol{R}}^{ij}}{F_{ii} + F_{jj} - \boldsymbol{\epsilon}_a^{ij} - \boldsymbol{\epsilon}_b^{ij}} \\ \bar{\mathbf{\Delta}}^{i} &= \frac{\bar{\boldsymbol{R}}^{ii}}{F_{ii} - \boldsymbol{\epsilon}_a^{ii}}. \end{aligned} \tag{5.19}$$

The increment is transformed back to the canonical basis,

$$\begin{aligned} \Delta^{ij} &= \boldsymbol{Q}^{ij}\boldsymbol{U}^{ij}\bar{\mathbf{\Delta}}^{ij}\boldsymbol{U}^{ij\dagger}\boldsymbol{Q}^{ij\dagger} \\ \Delta^{ii} &= \boldsymbol{Q}^{ii}\boldsymbol{U}^{ii}\bar{\mathbf{\Delta}}^{ii}\boldsymbol{U}^{ii\dagger}\boldsymbol{Q}^{ii\dagger} \end{aligned} \tag{5.20}$$

and added to the amplitudes of the previous iteration $(n-1)$,

$$\begin{aligned} t^{ij}(n) &= t^{ij}(n-1) + \Delta^{ij} \\ t^{i}(n) &= t^{i}(n-1) + \Delta^{i}. \end{aligned} \tag{5.21}$$

It should be noted that this procedure is applied for filtering the non-local parts of $\hat{T}$, $\hat{\Lambda}$, X_ω^A and Y_ω^A amplitudes.

5.4 Results and Discussions

5.4.1 $(H_2)_n$ Helices

First thing would be showing the retention of diffuse space. show the two graphs showing for (h2)7 systems. name it PNO(M) for modified PNO, mention that this is not feasible as big number of diffuse-functions, plus not a blackbox way for selecting the cutoff for retention. - Linear structure, chiral, helical arrangement - best case for local correlation problems - small

masses, high OR - Polariz, specific rotation (h2)4, (h2)5, (h2)6, (h2)7, maybe-bigger!! : LG, MVG, aDZ basis - diagnostics for FVNO++ approach: - first comparing the structure of the ground state and perturbed density, one can see that perturbed density would have a higher rank than ground-state density. - how about incorporating L*L density as well and optimized NOs by better guess densities. - Here we mostly concentrate on capturing the right kind of behavior rather than savings, since there is not enough sparsity on offer for these cases. This is applicable for other test cases as well.

5.4.2 beta-pinene

5.4.3 phenyl-ethanol

5.4.4 norbornenone

5.5 Conclusions

Chapter 6

Conclusions

Bibliography

[1] M. L. Abrams and C. D. Sherrill. Natural orbitals as substitutes for optimized orbitals in complete active space wavefunctions. *Chem. Phys. Lett.*, 395:227–232, 2004.

[2] R. Ahlrichs, H. Lischka, V. Staemmler, and W. Kutzelnigg. Pno-ci (pair natural orbital configuration interaction) and cepa-pno (coupled electron pair approximation with pair natural orbitals) calculations of molecular systems. i. outline of the method for closed shell states. *J. Phys. Chem.*, 62(4):1225–1234, February 1975.

[3] Fumihiko Aiga and Reikichi Itoh. Calculation of frequency-dependent polarizabilities and hyperpolarizabilities by the second-order moller-plesset perturbation theory. *Chem. Phys. Lett.*, 251:372–380, 1996.

[4] T. L. Barr and E. R. Davidson. Nature of the configuration-interaction method in *ab initio* calculations. i. ne ground state. *Phys. Rev. A*, 1(3):644–658, 1970.

[5] Rodney J. Bartlett and Monika Musial. Coupled-cluster theory in quantum chemistry. *Rev. Mod. Phys.*, 79:291, 2007.

[6] A. D. Becke. Density-functional thermochemistry. iii. the role of exact exchange. *J. Chem. Phys.*, 98(7):5648–5652, April 1993.

[7] C. F. Bender and E. R. Davidson. Studies in configuration interaction: The first-row diatomic hydrides. *Phys. Rev.*, 183(1):23–30, 1969.

[8] Max Born and J. Robert Oppenheimer. Zur quantentheorie der molekeln [on the quantum theory of molecules]. *Annalen der Physik (in German)*, 389(20):457–484, 1927.

[9] James R. Cheeseman, Michael J. Frisch, Frank J. Devlin, and Philip J. Stephens. Hartree-fock and density functional theory ab initio calculation of optical rotation using giaos: Basis set dependence. *J. Phys. Chem. A*, 104:1039–1046, November 1999.

[10] O. Christiansen, P. Jørgensen, and C. Hättig. Response functions from fourier component variational perturbation theory applied to a time-averaged quasienergy. *Int. J. Quantum Chem.*, 68:1–52, 1998.

[11] O. Christiansen, H. Koch, and Poul Jørgensen. The second-order approximate coupled cluster singles and doubles model cc2. *Chem. Phys. Lett.*, 243(5-6):409–418, September 1995.

[12] T. D. Crawford. Reduced-scaling coupled-cluster theory for response properties of large molecules. In P. Carsky, J. Pittner, and J. Paldus, editors, *Recent Progress in Coupled Cluster Methods: Theory and Applications*, volume 11 of *Challenges and Advances in Computational Chemistry and Physics*, chapter 2, pages 37–55. Springer, Berlin, 2010.

[13] T. D. Crawford and H. F. Schaefer. An introduction to coupled cluster theory for computational chemists. In K. B. Lipkowitz and D. B. Boyd, editors, *Reviews in Computational Chemistry*, volume 14, chapter 2, pages 33–136. VCH Publishers, New York, 2000.

[14] T. Daniel Crawford. Ab initio calculation of molecular chiroptical properties. *Theor. Chem. Acc.*, 115:227–245, December 2006.

[15] T. Daniel Crawford and Henry F. Schaefer. An introduction to coupled cluster theory for computational chemists. *Reviews in Computational Chemistry*, 14:33–136, 2000.

[16] Paul N Day, Jan H. Jensen, Mark S. Gordon, Simon P. Webb, Walter J. Stevens, Morris Krauss, David Garmer, Harold Basch, and Drora Cohen. An effective fragment method for modeling solvent effects in quantum mechanical calculations. *J. Chem. Phys.*, 105(5):1968–1986, 1996.

[17] A. E. DePrince and C. D. Sherrill. Accuracy and efficiency of coupled-cluster theory using density fitting/cholesky decomposition, frozen natural orbitals, and a t_1-transformed hamiltonian. *J. Chem. Theory. Comp.*, 9:2687–2696, 2013.

[18] A. E. DePrince and C. D. Sherrill. Accurate noncovalent interaction energies using truncated basis sets based on frozen natural orbitals. *J. Chem. Theory Comput.*, 9:293–299, 2013.

[19] T. H. Dunning. Gaussian basis sets for use in correlated molecular calculations. i. the atoms boron through neon. *J. Chem. Phys.*, 90(2):1007, 1989.

[20] C. Edmiston and M. Krauss. Pseudonatural orbitals as a basis for the superposition of configurations. i. he_2^+. *J. Chem. Phys.*, 45(5):1833–1839, 1966.

[21] J. T. Fermann, C. D¿ Sherrill, T. D. Crawford, and H. F. Schaefer. Benchmark studies of electron correlation in six-electron systems. *J. Chem. Phys.*, 100:8132–8139, 1994.

[22] R.P. Feynman. Forces in molecules. *Physical review*, 56:340–343, 1939.

[23] J. Friedrich, H. R. McAlexander, A. Kumar, and T. D. Crawford. Incremental evaluation of coupled cluster dipole polarizabilities. *Phys. Chem. Chem. Phys.*, 17:14284–14296, 2015.

[24] J. Gauss. The coupled-cluster method. In P.v.R. Schleyer, N. L. Allinger, T. Clark, J. Gasteiger, P. A. Kollman, H. F. Schaefer III, and P. R. Schreiner, editors, *Encyclopedia of Computational Chemistry*, pages 615–636. John Wiley and Sons, Chichester, 1998.

[25] Christof Hattig and Bernd Artur Hebeta. correlated frequency-dependent polarizabilities and dispersion coefficients in the time-dependent second-order moller-plesset approximation. *Chem. Phys. Lett.*, 233:359–370, 1995.

[26] T. Helgaker, S. Coriani, P. Jørgensen, K. Kristensen, J. Olsen, and K. Ruud. Recent advances in wave function-based methods of molecular -property calculations. *Chem. Rev.*, 112:543–631, 2012.

[27] H. J. Aa. Jensen, Poul. Jorgensen, H. Agren, and Jeppe Olsen. Secondorder moller–plesset perturbation theory as a configuration and orbital generator in multiconfiguration selfconsistent field calculations. *J. Chem. Phys.*, 88:3834, November 1988.

[28] P. Jorgensen and J. Simons. *Second Quantization-Based Methods in Quantum Chemistry.* Academic Press, New York, 1981.

[29] R. A. Kendall, T. H. Dunning, and R. J. Harrison. Electron affinities of the first-row atoms revisited. systematic basis sets and wave functions. *J. Chem. Phys.*, 96(9):6796–6806, 1992.

[30] Rika Kobayashi, Henrik Koch, and Poul Jørgensen. Calculation of frequency-dependent polarizabilities using coupled-cluster response theory. *Chem. Phys. Lett.*, 219:30–35, March 1994.

[31] H. Koch, R. Kobayashi, and P. Jørgensen. Brueckner coupled cluster response functions. *Int. J. Quantum Chem.*, 49:835, 1994.

[32] Henrik Koch and Poul Jørgensen. Coupled cluster response functions. *J. Chem. Phys.*, 93(5):3333–3344, September 1990.

[33] Rama K. Kondru, Peter Wibf, and David N. Beratan. Structural and conformational dependence of optical rotation angles. *J. Phys. Chem. A*, 103(33):6603–6611, 1999.

[34] Tatiana Korona, Klaus Pflüger, and Hans-Joachim Werner. The effect of local approximations in coupled-cluster wave functions on dipole moments and static dipole polarizabilities. *Phys. Chem. Chem. Phys.*, 6:2059–2065, March 2004.

[35] A. Landau, K. Khistyaev, S. Dolgikh, and A. I. Krylov. Frozen natural orbitals for ionized states within equation-of-motion coupled-cluster formalism. *J. Chem. Phys.*, 132:014109, 2010.

[36] C. Lee, W. Yang, and R. G. Parr. Development of the colle-salvetti correlation-energy formula into a functional of the electron density. *Phys. Rev. B.*, 37:785–789, 1988.

[37] P. O. Lowdin. Quantum theory of many-particle systems. i. physical interpretations by means of density matrices, natural spin-orbitals, and convergence problems in the method of configurational interaction. *Physical review*, 97(6):1474, March 1955.

[38] T. J. Mach and T. D. Crawford. Computing optical rotation via an n-body approach. *Theor. Chem. Acc.*, 133:1449, 2014.

[39] H. R. McAlexander and T. D. Crawford. A comparison of three approaches to the reduced-scaling coupled cluster treatment of non-resonant molecular response properties. *J. Chem. Theory Comp.*, 12(1):209–222, 2016.

[40] Harley R. McAlexander, Taylor J. Mach, and T. Daniel Crawford. Localized optimized orbitals, coupled cluster theory, and chiroptical response properties. *Phys. Chem. Chem. Phys.*, pages 7830–7836, 2012.

[41] Benedetta Mennucci, Jacopo Tomasi, Roberto Cammi, James R. Cheeseman, Michael J. Frisch, Frank J. Devlin, S. Gabriel, and Philip J. Stephens. Polarizable continuum model (pcm) calculations of solvent effects on optical rotations of chiral molecules. *J. Phys. Chem. A*, 106(25):6102–6113, May 2002.

[42] E. Merzbacher. *Quantum Mechanics,2nd ed.* Wiley, New York, 1970.

[43] Wilfried Meyer. Pnoci studies of electron correlatione ffects. i. configuration expansion by means of nonorthogonal orbitals, and application to the ground state and ionized states of methane. *J. Chem. Phys.*, 58(3):1017–1035, February 1973.

[44] Frank Neese, Frank Wennmohs, and Andreas Hansen. Efficient and accurate local approximations to coupled-electron pair approaches: An attempt to revive the pair natural orbital method. *J. Chem. Phys.*, 130(114108):114108–1 – 114108–18, 2009.

[45] Johannes Neugebauer. On the calculation of general response properties in subsystem density functional theory. *J. Chem. Phys.*, page 084104, 2009.

[46] Johannes Neugebauer, M. J. Louwerse, E. J. Baerends, and Tomasz Adam Wesolowski. The merits of the frozen-density embedding scheme to model solvatochromatic shifts. *J. Chem. Phys.*, 122:094115, 2005.

[47] Jeppe Olsen and Poul Jorgensen. *J. Chem. Phys.*, 82:3235, 1985.

[48] Thomas Bondo Pedersen and Berta Fernandez. Gauge invariant coupled cluster response theory using optimized nonorthogonal orbitals. *J. Chem. Phys.*, 114(16):6983–6993, February 2001.

[49] Thomas Bondo Pedersen, Henrik Koch, Linus Boman, and Alfredo M.J. Sanchez de Meras. Origin invariant calculation of optical rotation without recourse to london orbitals. *Chem. Phys. Lett.*, 393:319–326, June 2004.

[50] Prasad L. Polavarapu. Ab initio molecular optical rotations and absolute configurations. *Mol. Phys.*, 91(3):551–554, November 1997.

[51] G. D. Purvis and R. J. Bartlett. A full coupled-cluster singles and doubles model: The inclusion of disconnected triples. *J. Chem. Phys.*, 76:1910–1918, 1982.

[52] Julia E. Rice and Nicholas C. Handy. The calculation of frequencydependent polarizabilities as pseudoenergy derivatives. *J. Chem. Phys.*, 94:4959, 1991.

[53] C. Riplinger, P. Pinski, U. Becker, E. F. Valeev, and F. Neese. Sparse maps — a systematic infrastructure for reduced-scaling electronic structure methods. ii. linear scaling domain based pair natural orbital coupled cluster theory. *J. Chem. Phys.*, 144:024109, 2016.

[54] L Rosenfeld. Quantenmechanische theorie der naturlichen optischen aktivitat von flussigkeiten und gasen. *Z Physik*, 52:161–174, 1929.

[55] Nicholas J. Russ and T. Daniel Crawford. Local correlation in coupled cluster calculations of molecular response properties. *Chem. Phys. Lett.*, 400:104–111, November 2004.

[56] Nicholas J. Russ and T. Daniel Crawford. Local correlation domains for coupled cluster theory: Optical rotations and magnetic-field perturbations. *Phys. Chem. Chem. Phys.*, 10:3345–3352, May 2008.

[57] Kenneth Ruud, Philip J. Stephens, Frank J. Devlin, Peter R. Taylor, James R. Cheeseman, and Michael J. Frisch. Coupled-cluster calculations of optical rotation. *Chem. Phys. Lett.*, 373:606–614, March 2003.

[58] Ervin Schrodinger. An undulatory theory of the mechanics of atoms and molecules. *Physical review*, 28(6):1049–1070, December 1926.

[59] I. Shavitt and R. J. Bartlett. *Many-Body Methods in Chemistry and Physics: MBPT and Coupled-Cluster Theory*. Cambridge University Press, Cambridge, 2009.

[60] Jun Shen, Zhuangfei Kou, Enhua Xu, and Shuhua Li. The coupled cluster singles, doubles, and a hybrid treatment of connected triples based on the split virtual orbitals. *J. Chem. Phys.*, 136:044101–1 – 044101–9, January 2012.

[61] C. D. Sherrill and H. F. Schaefer. The configuration interaction method: Advances in highly correlated approaches. *Adv. Quantum Chem.*, 34:143–269, 1999.

[62] C. Sosa, J. Geertsen, G. W. Trucks, R. J. Bartlett, and J. A. Franz. Selection of the reduced virtual space for correlated calculations. an application to the energy and dipole moment of h_2o. *Chem. Phys. Lett.*, 159(2,3):148–154, 1989.

[63] P. J. Stephens, F. J. Devlin, C. F. Chabalowski, and M. J. Frisch. *Ab initio* calculation of vibrational absorption and circular dichroism spectra using density functional theory. *J. Phys. Chem.*, 98(45):11623–11627, 1994.

[64] Philip J. Stephens, Frank J. Devlin, James R. Cheeseman, and Michael J. Frisch. Calculation of optical rotation using density functional theory. *J. Phys. Chem. A*, 105:5356–5371, May 2001.

[65] Attila Szabo and Neil S. Ostlund. *Modern Quantum Chemistry: Introduction to Advanced Electronic Structure Theory*. Dover Publications, Inc., Mineola, New York, 1996.

[66] A. G. Taube and R. J. Bartlett. Frozen natural orbitals: Systematic basis set truncation for coupled-cluster theory. *Coll. Czech. Chem. Commun.*, 70(6):837–850, 2005.

[67] Andrew G. Taube and Rodney J. Bartlett. Frozen natural orbital coupled-cluster theory: Forces and application to decomposition of nitroethane. *J. Chem. Phys.*, 128(164101):164101–1 – 161101–17, April 2008.

[68] Jacopo Tomasi, Benedetta Mennucci, and Roberto Cammi. Quantum mechanical continuum solvation models. *Chem. Rev.*, 105(8):2999–3093, July 2005.

[69] Justin M. Turney, Andrew C. Simmonett, Robert M. Parrish, Edward G. Hohenstein, Francesco A. Evangelista, J. T. Fermann, Benjamin J. Mintz, Lori A. Burns, Jeremiah J. Wilke, Micah L. Abrams, Nicholas J. Russ, Matthew L. Leininger, Curtis L. Janssen, Edward T. Seidl, Wesley D. Allen, Henry F. Schaefer, Rollin A. King, Edward. F. Valeev, C. David Sherrill, and T. Daniel Crawford. Psi4: an opensource ab initio electronic structure program. *WIREs. Comput. Mol. Sci.*, 2:556–565, 2012.

[70] G.C. Wick. The evaluation of the collision matrix. *Physical review*, 80(2):268–272, October 1950.

[71] D. E. Woon and T. H. Dunning. Gaussian basis sets for use in correlated molecular calculations. iv. calculation of static electrical response properties. *J. Chem. Phys.*, 100(4):2975–2988, 1994.